An Experimental Investigation of Flow Energy Losses in Open-Channel Expansions

Azita Najafi-Nejad-Nasser

A Thesis

In

The Department

Of

Building, Civil, and Environmental Engineering

Presented in Partial Fulfilment of the Requirements

For the Degree of Master of Applied Science in Civil Engineering at

Concordia University

Winter 2011

CONCORDIA UNIVERSITY
School of Graduate Studies

This is to certify that the thesis prepared

By: A.Najafi Nejad Nasser _____

Entitled: _____

and submitted in partial fulfillment of the requirements for the degree of

_____

complies with the regulations of the University and meets the accepted standards with respect to originality and quality.

Signed by the final examining committee:

Dr. A.S. Ramamurthy
_____ Chair

Dr. S. Rakheja, MIE, External-to-Program
_____ Examiner

Dr. M. Zaheeruddin
_____ Examiner

Dr. S. Li
_____ Supervisor

Dr. M. Zaheeruddin
Approved by _____
Chair of Department or Graduate Program Director

Dr. Robin A.L. Drew
_____
Dean of Faculty

Date _____

ABSTRACT

An Experimental Investigation of Flow Energy Losses in Open-Channel Expansions
Azita Najafi-Nejad-Nasser

Channel expansions are common in both natural and engineered open channels. They connect a relatively narrow upstream section of channel with a large downstream section of channel. Due to increasing cross-sectional dimensions in an expansion, the flow decelerates. Under steady flow conditions flow deceleration results in an increase in water pressure and hence an adverse pressure gradient. This often triggers flow separation and turbulent eddy motion, and causes energy losses in the flow. When conservation of flow energy is required, the issue of energy losses becomes important, a consideration which has motivated this study. The focus of this study is on subcritical flow, a typical flow seen under a wide range of flow conditions. This study aims to quantify the energy losses in a lateral expansion and to further investigate how effective a hump fitted on the channel-bed of the expansion is at reducing energy losses.

This study adopted the experimental approach. Using a recirculating laboratory flume, experiments of flow in expansions with or without a hump were performed to measure flow depth, pressure, and cross-sectional mean velocities. These measurements were analysed using the energy concept for direct estimates of the energy loss coefficient. Without the hump, measured water pressures showed adverse gradient in the expansion, opposing the approaching flow. Estimates of the energy loss coefficients ranged from 0.46 to 0.62. These results would be useful for the design of channel expansions, and for calibrating and validating numerical

hydrodynamics models. The presence of the hump has been shown to accelerate the flow, convert adverse to favourable pressure gradient, and lower the energy loss coefficients by more than 50% when compared with the corresponding values without the hump.

So far no satisfactory theory has been established for determining the energy loss coefficient for a given expansion. In this study, the momentum concept is combined with the energy concept in order to derive a theoretical expression for the energy loss coefficient. When applying the momentum concept to flow in an expansion, the pressure forces may be evaluated using the hydrostatic approximation, as supported by experimental evidence from this study. The theoretical expression involves extra parameters whose values are obtained based on the experimental data. It has been shown that the theoretical and experimental values for the energy loss coefficient are in good agreement. This theoretical expression can easily be extended to study channel expansions of different configurations.

ACKNOWLEDGEMENT

In the first place I would like to express my gratitude to my supervisor, Dr Samuel Li. His guidance, encouragement and support throughout the research are greatly appreciated. His abundant help and invaluable assistance, support and guidance in preparing my thesis, are especially appreciated. I am truly fortunate to have such an excellent supervisor.

I also would like to thank Dr. A. S. Ramamurthy for the kindly provided the design drawings of the channel expansions.

I am especially thankful to Mr. Lang Vo for his help in installing the experiment setup.

Last but not least, I would like to thank my parents for their endless love and support through the whole duration of my studies.

TABLE of CONTENTS

LIST of FIGURES

LIST of TABLES

LIST OF SYMBOLS

A = Area

b_1 = upstream channel section width, CS 1

b_2 = channel width at CS 2

b_3 = channel width at CS 3

C_d = coefficient of discharge

D = hydraulic depth

E_1 = specific energy at CS 1

F_i = pressure force at cross section i

Fr_1 = Froude number of CS 1

F_w = reaction force of sidewall

g = gravity

H = head measured above the weir crest

H_i = total energy head

h = vertical distance between the water surface and the point of interest

h_L = energy loss in the expansion

h_f = energy loss caused by friction

h_e = energy loss, due to flow separation and eddy motion

k_E = energy loss coefficient

k_h = head correction factor

L_1 = upstream channel section length

L_2 = channel expansion length

L_3 = downstream channel section length

l = coordinate measured from CS 2, along the sidewall between cross sections CS 2 and CS 3

m = side slope of a trapezoidal channel (1:m)

n = Manning's coefficient

p = measured pressure

P = height of the crest of the V-notch

p_o = cubic equation parameters

p_h = hydrostatic pressure

p_L and p_R = pressures measured at the corresponding pressure openings on the sidewall

Q = total discharge

Q_o = cubic equation solutions

$\overline{Q_{vm}}$ = average of discharges by the volumetric method

$\overline{Q_{vn}}$ = average of the V-notch discharges

q_i (i = 1 or 3) = per-unit-width discharge

Re = Reynolds number

R_h = hydraulic radius

r = width ratio of b_2 to b_3

S = channel bottom slope

T = temperature or top width of the channel

v = flow velocity

v_1 = cross-sectional mean flow velocity at CS 1

v_2 = cross-sectional mean flow velocity at CS 2

y_f = observed final water-surface elevation, above an arbitrary datum

y_i = initial water-surface elevation, above an arbitrary datum

y = depth of flow

y_1 = depth of flow upstream of the expansion or at CS 1

y_2 = depth of flow at the entrance to the expansion or at CS 2

y_3 = flow depth at CS 3, where there are combination of the expansion

y_3* = dimensionless depth of flow $y_3^*(= y_3 / y_2)$

y_{3e} = flow depth at CS 3, where there is a pure expansion with a horizontal bottom

y_{3h} = flow depth at CS 3, where there is a hump in a channel of constant width

z_1 = elevation of the channel bottom at CS 1 above an arbitrarily chosen datum

z_2 = elevation of the channel bottom at CS 2 above the datum

ρ = density of fluid

α = divergence angle of the expansion

β_o = cubic equation parameters

γ = specific weight

ΔH = energy head saved

ΔL = distance between every two adjacent pressure openings along each row

Δp = deviation of the measured pressure, p, from the hydrostatic pressure, p_h

$\Delta z = z_3 - z_1$ = Elevation difference

Δz_{max} = maximum allowable elevation difference

δ = height of the hump

ε = angle of the bottom of the expansion with hump in the horizontal direction

η = water surface measured above the channel bottom

$\eta^* =$ dimensionless parameter $\dfrac{\eta(\xi)}{y_2}$

$\theta =$ V-notch angle

$\mu =$ dynamic viscosity of water

$\xi =$ middle point along the length of the expansion sidewall

Chapter One   Introduction

1.1   The Need for Knowledge

A channel transition is defined as a change in the direction of channel, the slope of bed level or cross-sectional area (Henderson 1966, p. 235). A more complicated case is the combination of the above-mentioned geometric features. Channel expansions are transitions with an increase in cross-sectional area in the direction of flow. They are commonly encountered in both natural open channels and constructed hydraulics facilities. Examples include flow through subdivided channels between bridge piers and water flowing out of culverts. Channel expansions are also common in laboratory flumes, aqueducts, tunnels and siphons.

Channel expansions are worth investigating because they disturb the approaching flow, and more importantly because they can cause significant energy losses. On one hand, the disturbances emerge locally in the expansion but persist much further downstream. On the other hand, the energy losses in expansions cannot be recovered. The issue of energy losses in expansion must be addressed if conservation of flow energy is required, as is the case under many circumstances.

In the case of a flow diversion channel for hydro-power generation, which often incorporates one or more expansions, the losses of flow energy in the expansions will mean less electrical power generated at the downstream hydro-power plant. In the case of irrigation channels with expansions, the losses of flow energy in the expansions will reduce the efficiency of the irrigation systems. The issue of flow energy losses in channel expansions is relevant and important in many other hydraulics engineering applications.

Open-channel flows are classified as supercritical flow, critical flow and subcritical flow, depending on the Froude number. Most of the time, it is subcritical flows that are generally

observed in open channels, including channel expansions. When passing through an expansion, the flow decelerates, with a rising water surface and a corresponding increase in pressure. This condition creates an adverse pressure gradient and potentially causes the main flow to separate from the sidewalls of the expansion. Consequently, eddies form locally in the corners of the expansion, but shear-induced turbulence can disturb the main flow over a large distance downstream.

Although the physical process of flow separation has attracted extensive research attention with impressive applications in many different fields, no satisfactory theory has been developed to determine the energy losses for a given channel expansion. The energy loss coefficient is almost always given assumed values, which are very likely to be subject to errors. There is a difficulty in using the energy principle because of an unknown amount of energy loss. A need exists for reliable estimates of the energy loss coefficient. This is essential for the proper design of hydraulics facilities involving expansions.

Given that flow separation in expansions is undesirable, is there any practical way to suppress flow separation? Can the energy losses in expansions be minimised? In the search for answers to these questions, a number of researchers have previously undertaken various approaches in their studies. However, most of the earlier studies have produced only qualitative results.

It is necessary to conduct detailed and quantitative investigations of flow behaviour and associated energy losses in a channel expansion. This study aims to satisfy this need by performing laboratory experiments of subcritical flows in an expansion in the Hydraulics Laboratory at Concordia University. This study represents an extension of the basic idea of using a simple hump fitted on the channel bottom of an expansion in order to reduce energy losses in

the field. The experimental data obtained can be analysed based on the momentum and energy concepts in a complementary manner.

1.2   Specific Aims of this Study

This study adopts the experimental approach, aiming to produce good amounts of flow and pressure measurements in a channel expansion under subcritical conditions, to predict the response of the flow to the changing channel geometry using the momentum principle, and to determine the energy losses by feeding the results from the momentum equation into the energy equation. The specific objectives of this study are as follows:

- Obtain measurements of water pressure, flow depth, cross-sectional mean flow velocity and water surface profile for the experiments.

- Determine the complete list of forces on the flowing water and perform momentum analysis for solutions of flow velocity and depth.

- Determine the energy losses and make comparisons between experiments with a lateral expansion and experiments with an extra hump fitted on the bottom of the expanding channel.

1.3   Scope of the Work

To achieve the objectives outlined above, the remainder of this thesis is divided into seven chapters.

Chapter 2 is a summary of the current state of knowledge pertinent to this study. This includes the progress made in the analysis of physical processes that are responsible for flow separation and the formation of turbulent eddies, conclusions about changes in flow velocity and

depth as well as energy losses occurring in an expansion with or without bottom variations, and other established facts concerning the design of hydraulically efficient channel expansions.

In Chapter 3, the theoretic background of flow in an expansion is presented in order to extend the study of subcritical flows in a quantitative manner. The momentum and energy principles are combined to derive analytical expressions for the determination of the energy loss coefficient. Numerical example calculations are provided to illustrate the calculation procedures.

Chapter 4 describes the experimental setup and experiment procedures for measurements of various flow variables. The descriptions include the design and assembly of the experiment facility, the plan of experiments using different flow rates and flow depths. Discussions are given about the key characteristics of the expansions as well as measurement devices used in this study.

Chapter 5 is devoted to presentation of the results for one set of experiments conducted using a channel expansion with a flat channel-bed. Analyses of the experimental data using the theoretical formulations presented in Chapter 3 are carried out. These involve the evaluations of all the forces for each of the experiments. Once the depth of flow at the downstream end of the expansion is determined, the energy loss relative to the velocity head at the upstream end of the expansion is obtained by using the energy principle. Direct comparisons are made between the theoretical and experimental results.

Chapter 6 presents the results for a new set of flow experiments using the same expansion as in Chapter 5 but with a hump fitted on the bottom of the expansion. The experimental data are analysed to show the advantages of the hump in regulating the flow, eliminating adverse pressure gradient and enhancing energy head recovery.

Finally, Chapter 7 provides discussions about how the hydraulic performance of channel expansions can be improved and how the flow energy analysis can be extended to expansions of other configurations. The experimental evidence and analytical results are summarised before conclusions are drawn. Suggestions for future research on the topic of the hydraulic performance of channel expansions are made.

Chapter Two   Selective Literature Review

2.1   Geometric Shape of Channel Expansions

Channel expansions may be classified into five different types: a cylindrical quadrant expansion, a straight line expansion, a square end expansion, a warped expansion, and a wedge expansion. These different expansions are illustrated in Figure 2.1. In a channel expansion, the expanding width in the horizontal may be accompanied by bed-level changes in the vertical. Hinds (1927) gave a summary of the empirical hydraulic design of transitions for flumes and siphons and made specific recommendations for various geometric shapes. The basic design objective is to achieve flow transition in a short distance with a minimum amount of flow disturbance.

In particular, Hinds (1927) provided details of a design method for expansions intended to connect a rectangular flume to a larger, trapezoidal downstream channel. The method begins with an assumed water-surface profile expressed by two reverse parabolas. The parabolas have equal length with an inflexion point at the middle between the inlet and outlet of the expansion and merge tangentially with the upstream and downstream water surfaces. For given hydraulic properties, including bottom slopes, total discharge and flume dimensions, the expanding width as a function of the distance from the inlet of the expansion is calculated using the energy principle, with an assumed value for the energy loss coefficient. Hinds (1927) recommended an S-curved warped wall expansion (Figure 2.1, "warped" type), which has received some popular opinion.

However, Smith and Yu (1966) found that the S-curved warped wall expansion recommended by Hinds (1927) was one of the least effective designs among the types of expansions that they tested. The problem with the recommended configuration was the occurrence of flow separation. Smith and Yu (1966) suggested that a straight walled diverging

expansion (Figure 2.1, "straight line" type) was more efficient than a curved wall expansion of the same length.

None of the expansions shown in Figure 2.1 involves variations in bed level along the length of the expansions. It is not surprising at all that there are practical cases where changes in bed level are required. Under such conditions, in order to describe the geometric shape of for example an S-curved warped wall expansion, it is necessary to obtain three functions with the distance from the inlet of the expansion as their argument. One of these three functions determines how the bed width varies non-linearly with the distance. Another function expresses the variation in bed level with the distance if the inlet and outlet of the expansion are at different elevations. The third function defines the progressive changes of sidewall slopes from vertical at the inlet to certain inclination at the outlet.
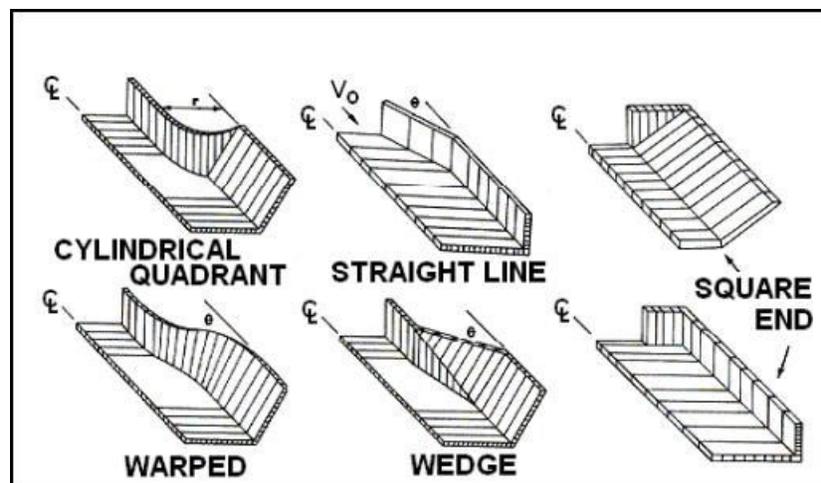
Figure 2.1   Channel expansion types (from U.S. Department of Transportation 1983, Chapter 4). All the expansions have geometry symmetric about the centreline.

2.2   Hydraulic Performance of Channel Expansions

In the absence of changes in bed level, as subcritical flow passes through an expansion the water surface will rise a vertical distance. Theoretically this vertical distance is equal to the reduction in velocity head between the inlet and outlet of the expansion. This is to say that there is a conversion of kinetic to potential energy. However, this conversion is accompanied by energy losses. Consequently, the actual rise of the water surface or the recovery of energy head is less than the theoretical vertical distance (Hinds 1927). A hydraulically efficient expansion means a conversion of as large a fraction as possible of the differential kinetic energy to potential energy. This is similar to the evaluation of the performance of diffusers (Reneau et al. 1967).

It is difficult to carry out mathematic analyses of flow energy for expansions of general geometry. So far no satisfactory theory for computing the energy losses in channel expansions has been proposed. A good alternative to characterise the energy losses would be to conduct experiments using expansions of widely used configurations, as shown in Figure 2.1. It is hoped that experimental results obtained for specific expansions can be extended to other expansions by e.g. careful interpolations.

Expansions may be classified as a sudden expansion (Figure 2.1, "Square end" type), a rapid expansion or a gradual expansion (Figure 2.1, all the types except the "Square end" type). A sudden expansion is one with an abrupt increase in channel width, say from b to B, where b is the width of the narrow upstream section of channel and B is the width of the wide downstream section of channel. Such an expansion is hydraulically poor (Henderson 1966, Chapter 7). This may be interpreted as lower rates of conversion of kinetic to potential energy.

Smith and Yu (1966) considered expansions as a rapid expansion when a total central angle, α, between sidewalls reached 28°10' or a 1:4 (Lateral:Longitudinal) rate of flare. A

gradual expansion may be considered as one with α values smaller than 28°10'. Flow separation is expected to occur when α increases to 19°10', corresponding to a 1:5.98 rate of flare, unless the width ratio $B/b < 2$ (Smith and Yu 1966). In flow separation zones, turbulent eddies form and cause energy dissipation in the flow. An attempt to avoid flow separation in an expansion by reducing α may not be practical under many instances, because the length required for the expansion will be excessively long and the cost to build such an expansion will be too high.

In fact, the assumption that perfection can be approached by reducing α is not necessary true. This has been illustrated in some examples given by Hinds (1927). A similar situation occurs in pipe flow in expanding pipes. Kalinske (1944) found that the loss of energy occurred more rapidly in the 30° expansion than in the sudden expansion. Instead of reducing α, Hinds (1927) emphasised the importance of giving careful attention to the design of detailed dimensions and forms of the expansion. The computed water-surface profile through the expansion shall be a smooth, continuous curve, approximately tangent to the water surface curves in the upstream and downstream sections of the channel, and shall not contain angular change in the water surface (Hinds 1927; Morris and Wiggert 1972, p. 185). It is important to make visual observations of the water surface profile during an experiment.

In summary, for the design of expansions the water-surface profile is computed using the energy principle. How accurate the computation is relies on more or less guessed energy losses. One ought to be cautious about considerable errors that the computational results may contain.

2.3   Streamline Patterns in Channel Expansions

Some earlier investigators of fluid flow in expansions have dealt with the limiting case of sudden expansions (see e.g. Abbott and Kline 1962; Mehta 1979, 1981; Graber 1982; Nashta and Garde

1988; Foumeny et al. 1996; Escudier et al. 2002). The results reported in their studies emphasised the effects of different expansion ratios on fluid pressure distributions, mean flow velocities, and turbulence characteristics. What is particularly important is the asymmetric behaviour of the flow field in perfectly symmetric expansions, first reported probably in Abbott and Kline (1962).

Flow separation can take place on either side of the expansion, with the maximum velocity line deviating from the centreline of the expansion. These were evidenced in the experimental data obtained by Smith and Yu (1966) and by Mehta (1979, 1981). Mehta (1981) showed that the mean flow patterns become more asymmetric and unsteady with increasing expansion ratios. Graber (1982) attributed the asymmetric flow behaviour to a static instability of a flow system. The stability analysis of Graber (1982) is subject the constraint that the Froude number is less than 0.2. This is a severe limitation because open-channel flows with the Froude number exceeding 0.2 are frequently observed. Based on numerical simulations of flow bifurcations, Foumeny et al. (1996) showed the existence of a value of the Reynolds number at which the flow downstream of the expansion became asymmetric.

So far one is not able to predict the onset of asymmetric flow patterns with certainty. Asymmetric flow patterns have consequences devastating to many hydraulic engineering structures. Smith and Yu (1966) observed in a rapid expansion that the flow from upstream followed one sidewall and large turbulent eddies appeared between the flowing jet and the other sidewall (Figure 2.2).
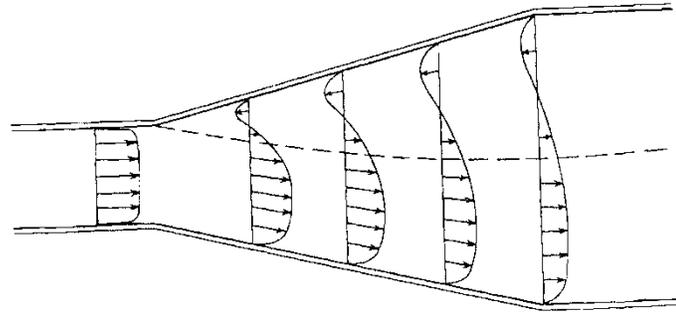
Figure 2.2   Plan view velocity distribution for a rapid expansion: B/b = 3.0 (Smith and Yu 1966).

Nashta and Garde (1988) did obtain head loss curves by fitting experimental data, but the data were from less common sudden expansion experiments. The head loss was expressed by the Borda-Carnot relationship, involving the velocity head, the depth of flow and the expansion ratio. The curves show variations in the energy loss coefficient with cross-sectional area. It is interesting to note that the analysis of Nashta and Garde (1988) included the energy loss due to friction in the total energy loss. However, are the geometric shape curves applicable to a gradual expansion? What is the role of the divergence angle which is not a parameter in sudden-expansions?

A number of investigators have made research efforts to improve the empirical S-curved warped wall expansion recommended by Hinds (1927) for connecting a rectangular flume with a trapezoidal downstream channel of larger cross section. The essential idea is to optimise the geometric shape of the expansion in order to achieve minimal energy losses in the expansions. The optimisation process makes use of the fundamental continuity and energy principles. The results are some modified boundary curves in the horizontal plane.

Using a rational method based on the concept of specific energy, Vittal and Chiranjeevi (1983) attempted to improve the geometric shape of the trapezoidal expansion. They proposed three functions to describe the bed width, bed elevation and sidewall slope, respectively. Swamee and Bask (1991) applied the optimal-control theory to improving the design of rectangular open-channel expansions. Swamee and Basak (1992) extended the application of the optimal-control theory to further improve the geometric shape of the trapezoidal expansion reported in Vittal and Chiranjeevi (1983). This extension achieved a marginal reduction to the energy losses compared with the values of Vittal and Chiranjeevi (1993). Swamee and Basak (1993) combined the design ideas presented in Swamee and Basak (1991, 1992). A common limitation of all the above-mentioned investigations is that the energy loss coefficient is assumed.

The idea of using a triangular sill in a channel expansion to suppress flow separation and eddy formation was first reported in Seetharamiah and Ramamurthy (1968). They simplified the problem by dropping an unknown amount of energy losses that would take place between the inlet and outlet of the expansion. This simplification allowed them to use the specific energy diagram to explain mechanics of the flow past the triangular sill. As subcritical flow passes over the sill, part of the flow energy head is stored as elevation.

As an extension to the work of Seetharamiah and Ramamurthy (1968), Ramamurthy et al. (1970) conducted experiments of subcritical flows passing gradual expansions. The flume used in the study was made of precast concrete slabs. Presumably, the sidewalls as well and the flume bottom had significant surface roughness. As a result, the factors that control flow changes in the expansions would include not only deceleration but also channel roughness. The fundamental momentum principle is still applicable. However, there is a difficulty about accurately incorporating the frictional forces associated with channel roughness into the momentum

equation. However, Ramamurthy et al. (1970) provided convincing experimental evidence that a hump fitted on the bottom was effective at reducing flow separation zones. The major results presented in the paper were velocity contours at a cross section at the crest of the hump. It would be useful to extend their work in order to obtain detailed measurements, including distributed pressures, and to quantify the reduction of energy losses in the flow.

The earlier investigations of subcritical flow in expansions have improved our understanding of the shape of separating streamline, deflection angle, the length of standing eddies and asymmetric behaviour. Although the improved understanding is useful to the optimal design of channel transitions, these investigations have not directly addressed the issue of flow energy losses in channel expansions.

2.4   Erodible Channel Expansions

So far it has assumed that the channels and expansions of interest are non-erodible. Under some circumstances, turbulent eddy motion in the flow separation zones can give rise to flow shear stress strong enough to erode the channel sidewalls and the channel bed. The process involves sediment transport and morphological change, which is very complex and difficult to predict.

Mohapatra and Bhalamudi (1994) considered the case where the bed level varied temporally in gradual channel expansions with an erodible bed. The authors used analytical and numerical models to obtain equilibrium solutions of the bed level variation in the expansions. Their work was limited to small expansion angles under steady conditions. The analytical and numerical models were based on the continuity and momentum principles, assuming that the flow depth and velocity did not vary across the channel width. This assumption would be

questionable, since the channel bed was mobile and inevitably varied across the channel (Smith and Yu, 1966).

2.5   Channel Contractions

For the sake of completeness, channel contractions are briefly discussed below. Relatively speaking, flow passing through a contraction suffers less from the problem of separation because streamlines are converging. However, a contraction may act as a choke for the upstream flow. In open channel design, choked flow is undesirable and should be prevented. The topic of preventing choked flow condition has been studied by a number of investigators. Liong (1984) analyzed the case of a rectangular channel, using the energy principle. The author used graphic solutions for one dimensional, steady, uniform flow without choke flow. Liong's (1984) analysis considers not only variations in channel width, but also variations in both channel width and channel-bed elevation.

Dey (1998) conducted a numerical study of flow through a circular transition, focusing on choke-free condition. The flow is subcritical upstream of the transition, whereas it is critical downstream of the transition. One-dimensional energy and continuity equations were used in Dey's (1998) numerical study. The main results are the maximum permissible limits of bed elevation rises and allowable ranges of the upstream flow depth.

2.6   Frictional effects

Bottom friction can have a significant influence on the flow in natural channel expansions. Babarrutsi et al. (1989) investigated experimentally the influence on re-circulating flows in a shallow open-channel expansion, and compared their experimental results with the field

measurements of island wakes made by Ingram and Chu (1987). The inclusion of bottom friction appeared to represent a better reflection of the reality. Specifically, Babarrutsi et al.'s (1989) velocity measurements showed that the bed friction caused both the length of the re-circulating zone and re-circulating flow rate to decrease. Babartutsi et al. (1991) repeated the same experiments but used dye technique in order to improve wake flow pattern visualisation. All the results reported were based on experiments with a sudden expansion.

The implication is that an experimental setup to investigate the effect of channel expansion on flow separation should be built using materials with insignificant roughness height. In this study, smooth-surfaced plexiglass is used to the channel sections and expansions. Energy losses due to surface friction are not expected to be significant.

2.7   Field measurements of subcritical flow in channel expansions

It would be constructive to make comparisons between experimental or analytical results and field measurements. A survey of the literature shows a very small number of field investigations of subcritical flows in channel expansions. Papanicolaou and Hilldale (2002) made Acoustic Doppler Velocimeter measurements of flow velocity at a channel cross section downstream of a channel expansion in a small creek. Their focus was on the spatial distributions of turbulent characteristics, including mean flow velocity, turbulent intensity and turbulent shear stress.

The results indicated that secondary flows were presented downstream of the expansion, and the flow field was anisotropic throughout the depth, with the transverse and vertical velocities changing direction. The channel expansion created an unbalanced or asymmetric turbulent shear stress distribution. Unfortunately, it is not possible to use the field observations

for flow energy calculations for two reasons. First, the measurements of flow velocity were made at a single cross section. Secondly, no measurements of flow depth were available.

2.8   Summary

In summary, gradual expansions are very common in both natural and engineered open channels. As a matter of fact, almost all natural open channels vary in width. Along the path of the channel flow, gradual expansions connect a narrow section of channel with a wide section of channel at downstream. When passing through an expansion, the flow is not expected to recover its original state before entering the expansion. The exact amount of flow energy lost in the expansion is unknown. A mechanism can be provided to suppress flow separation from the channel sidewalls and hence to minimise the formation of turbulent eddies in separation zones. Earlier investigators have made an impressive progress. However, much more research efforts are needed for detailed, quantitative results.

Chapter Three   Theoretical Background

3.1   Introduction

Chapter 2 provided a review of previous studies of steady flows in a channel expansion. Although earlier research took various approaches such as laboratory experiments, field measurements and theoretical analyses, research attention was restricted mostly to qualitative descriptions of the flow behaviour. In this chapter, relevant fundamental principles are presented as a basis to extend the study of flows in a channel transition in a quantitative manner. This begins in Section 3.2 with the description of the energy principle pertinent to open-channel flows in a flat-bottom expansion. Section 3.3 discusses the energy principle for flow in an open-channel with bottom variations. Section 3.4 extends the discussion to include the effect of incorporating a hump on the bottom.

Energy loss is expected to occur in the expansion, which must be included in the energy balance equation. In fact, there is a lack of prior knowledge of this energy loss, therefore it is difficult to directly apply the energy principle for solutions to the problem of open-channel flows in an expansion. This situation is very similar to the problem of hydraulic jumps. The problem of flows in an expansion can be tackled by using the momentum principle. This limit is discussed in Section 3.5.

In preparation of applying the momentum principle, Section 3.6 treats all the forces. The discussion of the momentum principle is taken up in Section 3.7. The momentum equation is normalised in Section 3.8. Once the state of the flow is determined from the momentum principle, one may find subsequently the energy loss in the expansion from the energy equation. The combination of the momentum and energy principles is done in Section 3.9.

3.2 **Energy Balance for Flows in a Pure Channel Expansion**

A pure channel expansion is here defined as a section of channel whose width increases monotonically in the direction of flow and where the channel bottom is flat. The plan view of such an expansion is schematically shown in Figure 3.1. The expansion is between cross sections CS 2 and CS 3. It connects a relatively narrow section of channel at the upstream with a wide section of channel at the downstream. In this study, all cross sections are considered to be of rectangular shape.

In the channel between cross sections CS 1 and CS 2, the energy equation is given by

$$y_1 + \frac{v_1^2}{2g} + z_1 = y_2 + \frac{v_2^2}{2g} + z_2 + h_f \qquad (3.1)$$

where y_1 is the depth of flow upstream of the expansion or at CS 1, v_1 is the cross-sectional mean flow velocity at CS 1, g is the gravity, z_1 is the elevation of the channel bottom at CS 1 above an arbitrarily chosen datum, y_2 is the depth of flow at the entrance to the expansion or at CS 2, v_2 is the cross-sectional mean flow velocity at CS 2, z_2 is the elevation of the channel bottom at CS 2 above the datum, and h_f is the energy loss incurring between the two cross sections due to friction at the channel bed and on the sidewalls.

The energy loss h_f is negligible, in the consideration that the channel bottom and sidewalls are smooth surfaces with a very low roughness and the longitudinal distance between cross sections CS 1 and CS 2 is short. The elevation terms z_1 and z_2 in Equation (3.1) can be eliminated by setting up the channel bottom at the same elevation between the two cross sections. Thus, Equation (3.1) is reduced to

$$y_1 + \frac{v_1^2}{2g} = y_2 + \frac{v_2^2}{2g} \qquad (3.2)$$

This equation simply states that the flow has the same specific energy at the two cross sections.

Plan View
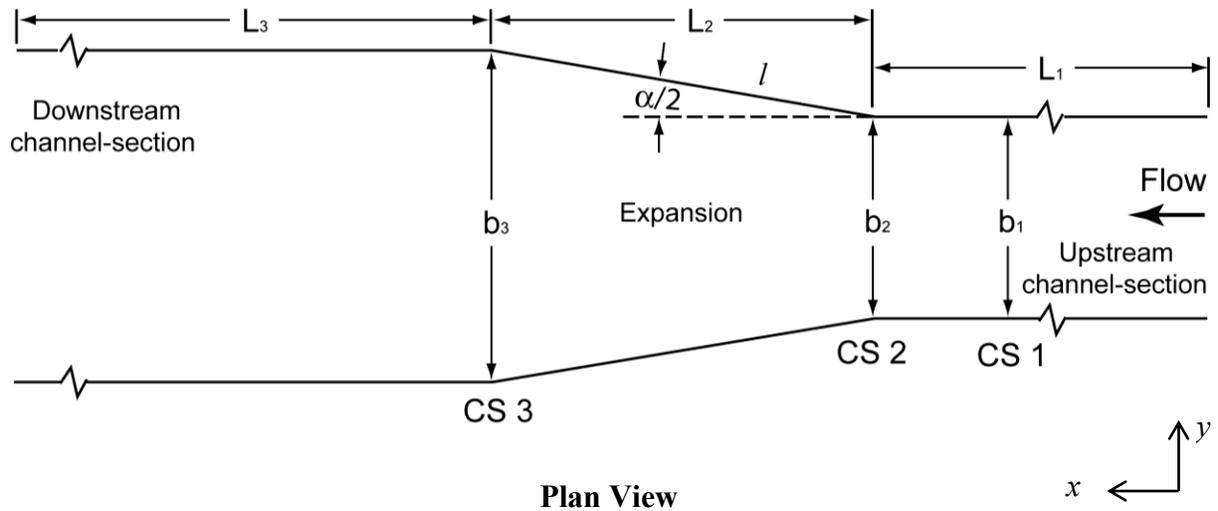
Figure 3.1   Definition diagram of a channel expansion, showing the length of the expansion and the lengths of the upstream and downstream channel-sections. The expansion has a divergence angle α, with its width changing from b_1 at its upstream end (CS 2) to b_3 at its downstream end (CS 3). The corners are blunt. The flow is from right to left.
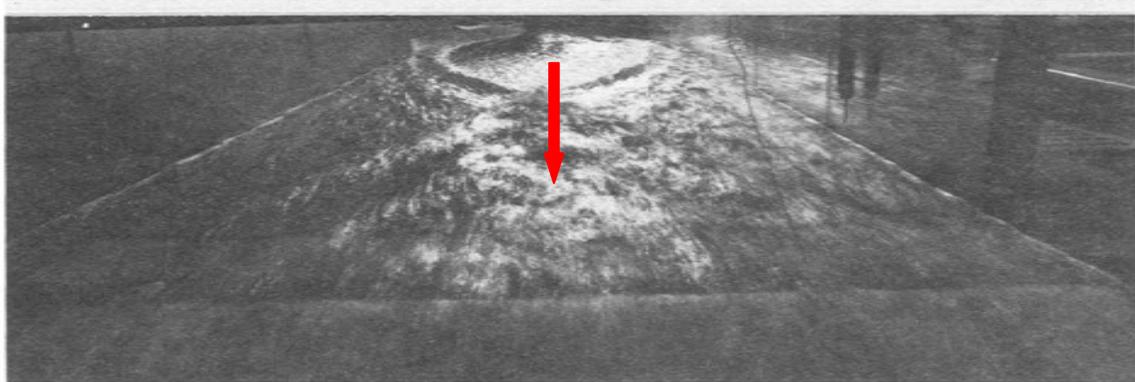
Figure 3.2   Visible shock waves emerging downstream of a channel expansion. The flow is from the top to the bottom, as indicated by the thick arrow. The flow approaching the expansion is supercritical with the Froude number greater than one (adopted from Mazumder and Hager, 1993).

In Equations (3.1) and (3.2) it has been assumed that the depth of flow is uniform in the cross-channel direction. This assumption entails great care on us to avoid the generation and propagation of surface waves of significant amplitude in the expansion during experiments. Strictly speaking, this may not be possible, in particular when the approaching flow is associated with high Froude number. The Froude number is defined as the ratio of flow velocity to the speed at which small-amplitude surface waves propagate. When evaluated at the upstream cross section or CS 1, the Froude number is given by

$$Fr_1 = \frac{v_1}{\sqrt{gy_1}} \tag{3.3}$$

where v_1 is the flow velocity at CS 1, g is the gravity and y_1 is the depth of flow at CS 1.

The situation of being disturbed by surface waves is worse for supercritical flow with the Froude number $Fr > 1$. Shock waves are inevitably generated in the expansion and perturb the flow over a distance many times the length of the expansion, as shown in Figure 3.2. The energy balance between cross sections CS 2 and CS 3 (Figure 3.1) is expressed as

$$y_2 + \frac{v_2^2}{2g} + z_2 = y_3 + \frac{v_3^2}{2g} + z_3 + h_L \tag{3.4}$$

where the subscript 3 is used for cross section CS 3. The last term h_L represents the energy loss in the expansion. This term consists of the energy loss caused by friction, the same as h_f in Equation (3.1), and the energy loss, h_e, due to flow separation and eddy motion (Henderson, 1966). The latter is greater by far than the former, i.e. $h_e \gg h_f$. Thus, h_L in Equation (3.4) may be approximated as

$$h_L \approx h_e \tag{3.5}$$

The state of knowledge concerning the physical process that governs flow separation and eddy motion is inadequate for accurate determination of the term h_e. Essentially, h_e is an unknown energy loss. Thus, it is not practical to directly apply the energy principle to the problem of open-channel flows in an expansion. In fact, the purpose of the energy analysis is to determine the energy loss h_e. This is done by incorporating Equations (3.2) and (3.5) into (3.4), and at the same time by using the equation of continuity. The resultant equation is given by

$$h_e = y_1 + \frac{q_1^2}{2gy_1^2} - (z_3 - z_1) - \left(y_3 + \frac{q_3^2}{2gy_3^2} \right) \tag{3.6}$$

Notice that the equation of continuity is of the form $u_1 = q_1 / y_1$ and $u_3 = q_3 / y_3$, where q_i ($i = 1$ or 3) is the per-unit-width discharge. This discharge is larger at cross section CS 1 than at cross section CS 3.

Equation (3.6) will be used to directly determine the energy loss dominantly due to flow separation and turbulent eddy motion in the expansion from measurements of the depth of flow at cross sections CS 1 and CS 3 (Figure 3.1). Notice that there is no need for measurements from the entrance cross section CS 2. In fact, it is more difficult to obtain accurate measurements at CS 2, because the flow there is subject to disturbances from surface waves to a larger extent than at the upstream cross section CS 1.

In the limit of zero energy loss in a horizontal channel, both $h_e = 0$ and $\Delta z = 0$. Equation (3.6) is reduced to a cubic equation for the depth of flow y_3 at the downstream end of the expansion or at CS 3

$$y_3^3 - \left(y_1 + \frac{q_1^2}{2gy_1^2} \right) y_3^2 + \frac{q_3^2}{2g} = 0 \tag{3.7}$$
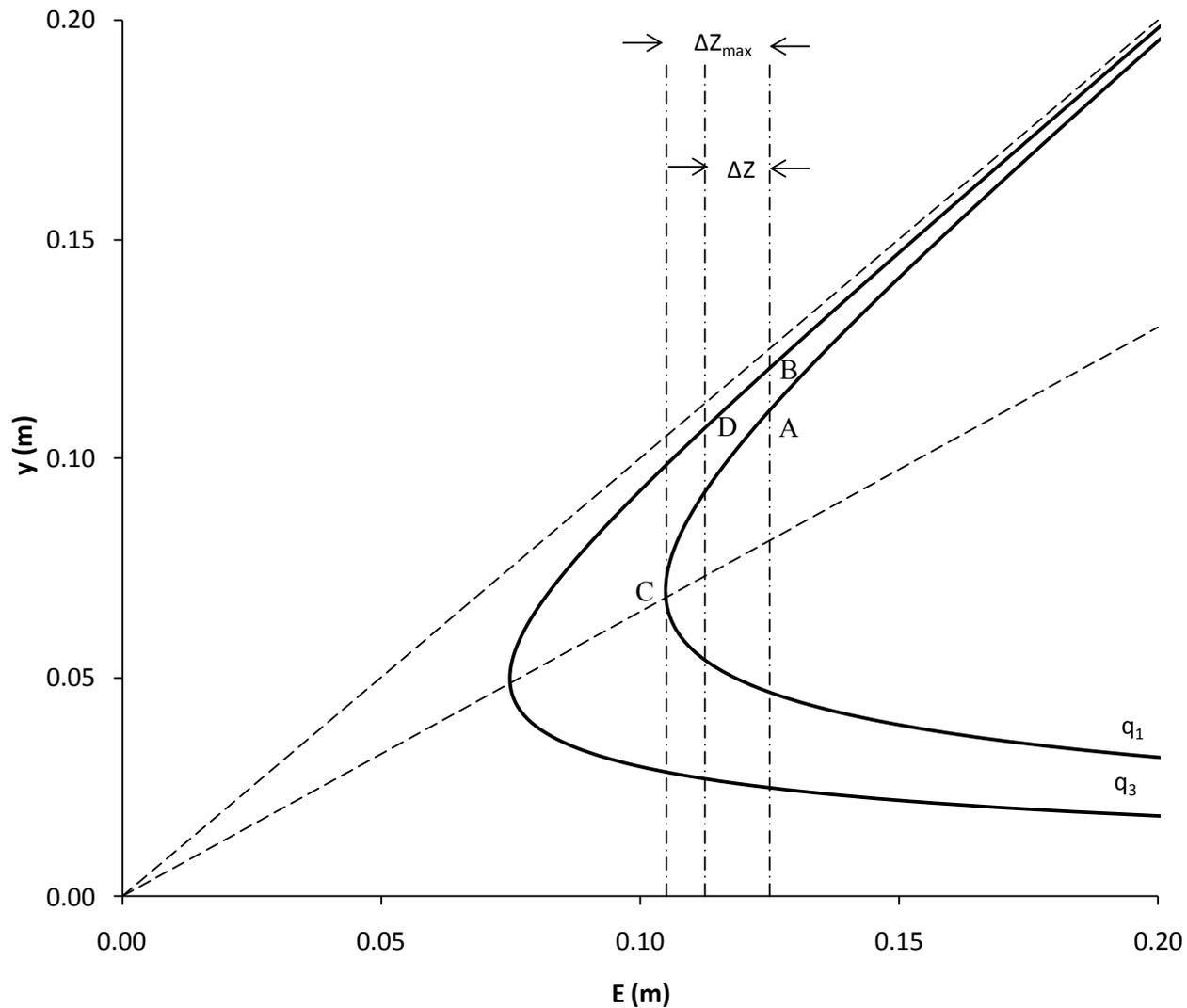
Figure 3.3   Specific energy diagram for flow in a channel expansion. The E-y curve to the right (the q_1 curve), shows all possible depths of flow and corresponding specific energry, with a per-unit-width discharge of q_1. The q_3 curve is similsr to the q_1 curve, but the per-unit-width discharge is $q_3 < q_1$. In the limit of zero energy loss in a horizontal channel, the depth of subcritivcal flow increases in the direction of the flow.

Elevation
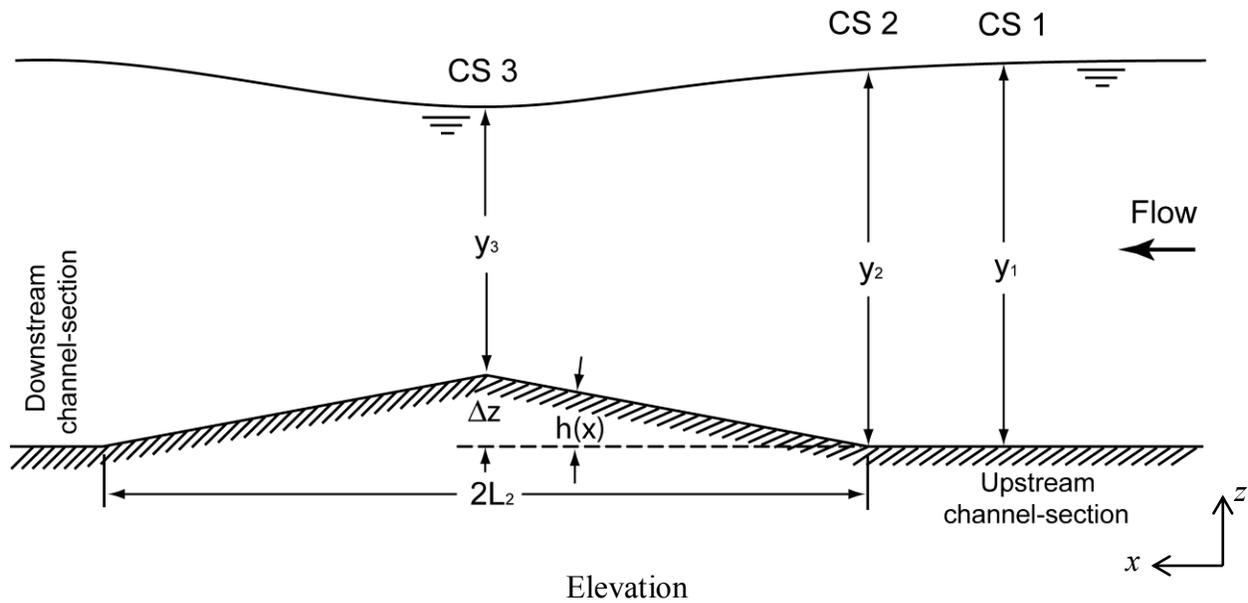
Figure 3.4   Water surface profile for flow over a hump fitted on the bottom of a uniform channel. From cross section CS 2 to cross section CS 3 the water pressure is decreasing while the flow accelerates up-slope. From CS 3 toward downstream the water pressure is increasing while the flow decelerates down-slope. On the basis of the energy principle, the depth of flow decreases over the hump.

This equation is discussed in many standard hydraulics textbooks (e.g. Chow, 1959; Henderson, 1966). Graphical solutions for y_3 can be obtained using the specific energy diagram (Figure 3.3). The procedures are described below.

Suppose that point A on the upper limb of the E-y curve to the right represents the subcritical flow of known depth y_1 and specific energy E_1, which approaches the expansion. A straight vertical line can be drawn through point A. This line intersects the upper limb of the E-y curve to the left at point B. The ordinate of point B gives the depth of flow at the downstream end of the expansion or at CS 3. The flow velocity at CS 3 can further be determined by using

the equation of continuity. It is interesting to note that the depth of subcritical flow in a channel expansion increases in the direction of the flow.

3.3   Energy Balance for Flows over a Hump in a Uniform Channel

Consider the case where the channel divergence angle α shown in Figure 3.1 is zero, and hence there is no variation in the per-unit-width discharge in the direction of flow, i.e. $q_3 = q_1$, but a hump ($\Delta z = z_3 - z_1$) is present on the channel bottom, as shown in Figure 3.4. With zero energy loss, Equation (3.6) becomes

$$y_3 + \frac{q_3^{\ 2}}{2gy_3^{\ 2}} + \Delta z = y_1 + \frac{q_1^{\ 2}}{2gy_1^{\ 2}} \qquad (3.8)$$

The effects of the hump on the flow can be examined using the above equation. Importantly, the elevation difference Δz must not be so large that the approaching flow is 'choked' (Henderson, 1966).

Suppose that point A on the upper limb of the E-y curve to the right in Figure 3.3 represents the subcritical flow that approaches the hump. The maximum allowable elevation difference is marked by Δz_{max}. This is the distance between the straight vertical line drawn through point A and the straight vertical line through point C that represents the condition of critical flow with the minimum specific energy for the given per-unit-width discharge.

For any given value of Δz smaller than the maximum allowable value Δz_{max}, at a horizontal distance of Δz to the left of the straight vertical line through point A, a straight vertical line can be drawn. This line intersects, at point D, with the upper limb of the same E-y curve on which point A is. The ordinate of point D gives the depth of flow over the hump. As shown in

Figure 3.3, the depth of flow decreases over the hump, relative to the depth of the approaching flow.

3.4   Energy Balance for Flows in an Expansion with a Hump Fitted on the Bottom

The previous two sections discussed the effects of expanding width and raising bottom on the flow separately. A channel expansion causes the depth of flow to increase in the direction of the flow, whereas the presence of a hump on the channel bottom causes the depth of flow to decrease. Now the case of combining a channel expansion, shown in Figure 3.1, with a hump fitted on the channel bottom, shown in Figure 3.4, will be studied by applying the energy principle in a series of sample calculations. It is understood that these sample calculations exclude the possibility that energy losses occur in the channel transition. Various parameters are given values more or less close the experiment conditions to be presented in later chapters.

A series of hypothetical values for the depth of flow y_1 at the upstream cross section CS 1 (Figure 3.1) in the range of 0.10 to 0.20 m are used in the sample calculations presented. A summary is given in Table 3.1. The per-unit-width discharge is $q_1 = 0.058$ m^2/s at the upstream cross section CS 1, and in the case of expanding channel, $q_3 = 0.035$ m^2/s at the downstream cross section CS 3. The crest of the hump is given a height of $\Delta z = 0.006$ m. The Froude number is evaluated at the upstream cross section CS 1 or $Fr = v_1 /(gy_1)^{1/2}$. For comparison purposes, the depth of flow at the downstream end of a pure channel expansion is calculated using Equation (3.6) and shown as y_{3e} in Table 3.1. The depth of flow over the hump of a uniform channel is calculated using Equation (3.8) and shown as y_{3h} in the table. The depth of flow y_3 at the downstream end of a channel expansion fitted with a hump on the channel bottom is calculated using Equation (3.6) with the energy loss h_e dropped.

The results from the sample calculations are summariesed in Table 3.1. In the first case where there is a flat-bottom expansion with a horizontal bottom (no hump), it can be seen that the depth of flow increases in the expanding channel, which is what is expected. The increases range from 1.01 to 1.12 times the depth of flow at cross section CS 2 (Figure 3.1). In the second case where there is a hump in a channel of constant width, the depth of flow decreases to 90% to 96% of the depth of flow at CS 2. This is also what is expected.

In the third case, the channel expansion of the first case is combined with the hump of the second case. The expanding width and the rising bottom work against each other. The former causes the flow to decelerate and the depth to increase, whereas the latter causes the flow to accelerate and the depth to decrease. The effect of the former appears to dominate that of the latter at high Froude numbers, whereas the opposite is true at low Froude numbers. We caution that these results correspond to the specific conditions that we have imposed on Q, q_1, q_3 and Δz, and should not be generalised without further systematic assessment.

Table 3.1   Calculated depth of flow at CS 3 using the energy concept. The depth ratio is given as $y_3{}^* = y_3/y_1$.

y_1 (cm)	10	12	14	16	18	20	22
Fr_1	0.59	0.45	0.35	0.29	0.24	0.21	0.18
y_{3e} (cm)	11.2	12.8	14.6	16.5	18.3	20.2	22.3
y_{3h} (cm)	9.0	11.2	13.3	15.4	17.3	19.3	21.4
y_3 (cm)	10.5	12.2	14.0	15.8	17.7	19.6	21.7
$y_3{}^*$	1.050	1.017	1.000	0.988	0.983	0.980	0.986

3.5   Limitations on the Use of the Energy Concept

Henderson (1966) highlighted major limitations on the use of the energy concept in open-channel flow. In the particular case of flow in a channel expansion, difficulty arises for two reasons. Firstly, an unknown energy loss is assumed as negligible, which cannot be true. Secondly, the velocity and depth will be uniform at the entire cross section immediately when the flow enters the expanded section. In reality, uniform conditions can only be established until a point is reached some distance downstream.

The momentum equation is most commonly used in situations where the energy equation is not applicable due to an unknown energy loss. The energy loss can be calculated from the energy equation after it is fed with the results from the momentum equation. The use of the momentum equation needs to include the complete list of all the forces.

3.6   Pressure and Sidewall Forces

For the block of fluid bounded by cross sections CS 2 and CS 3 (Figure 3.1), the complete list of forces includes the pressure force F_2 at cross section 2 and the pressure force F_3 at cross section 3, and the force F_w exerted by the contacting channel sidewalls on the flowing water. Assume that the pressure forces F_2 and F_3 are hydrostatic. The two forces are related to the depth of flow at the two cross sections as

$$F_2 = \frac{1}{2}\rho g b_2 y_2{}^2 \tag{3.9}$$

$$F_3 = \frac{1}{2}\rho g b_3 y_3{}^2 \tag{3.10}$$

where b_2 is the channel width at CS 2, and b_3 is the channel width at CS 3 (Figure 3.1).

It is further assumed that the sidewalls of the expansion are subject to hydrostatic pressure force exerted by the flowing fluid. The reaction force, F_w, is obtained by integrating the hydrostatic pressure, p, over the area, A, of one of the sidewalls of the expansion or $F_w = \iint p dA$. This integral is evaluated as

$$F_w = \rho g \int_0^{L_2/\cos(\alpha/2)} \int_0^{\eta} y\,dy\,dl \qquad (3.11)$$

where η is the water surface measured above the channel bottom, y is the depth below the water surface, l is the coordinate measured from cross section 2 (Figure 3.1) along the sidewall between cross sections 2 (CS 2) and 3 (CS 3), and L_2 is the distance along the sidewall between the two cross sections. The Integrating over y yields

$$F_w = \frac{1}{2}\rho g \int_0^{L_2/\cos(\alpha/2)} \eta^2 dl \qquad (3.12)$$

Notice that $\eta(l)$ varies along the sidewall between the two cross sections. Its dependent variables presumably include the divergence angle, α, the Froude number, Fr_1, and the Reynolds number of the flow that approaches the expansion from upstream.

There is a lack of knowledge about the functional form of η for us to proceed to evaluate the integral in Equation (3.12). However, according to the Mean Value Theorem for integrals, some ξ exists in the closed interval joining cross sections CS2 and CS3 such that

$$F_w = \frac{\rho g L_2}{2\cos(\alpha/2)}\eta(\xi)^2 \qquad (3.13)$$

where the integrand, η^2, is considered continuous on the closed interval. The simplest choice of ξ will be the middle point along the length of the expansion sidewall. The experiments reported in

this study provide data for the evaluation of F_w using the integral form in Equation (3.12) and the algebraic form in Equation (3.13).

3.7 Momentum Equation

Consider the section of fluid bounded by CS2, CS3 and the channel sidewalls, shown below
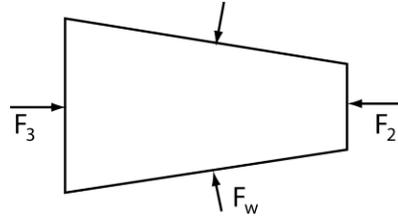
Figure 3.5 Free body diagram for momentum analysis.

In the direction of the flow, the momentum equation is given by

$$F_2 - F_3 + 2\sin\left(\frac{\alpha}{2}\right)F_w = \rho Q(v_3 - v_2)$$

(3.14)

where ρ is the density of fluid and Q is the total discharge. The sum of the three forces on the left hand side of the equation acts on the block of fluid and results in a change of its momentum given on the right hand side. Multiplying F_w by $\sin(\alpha/2)$ resolves the force into the direction of the mean flow. Viscous forces on the channel bottom and sidewalls have been neglected.

A sudden expansion corresponds to $\alpha = 180°$. In this special case, the momentum equation becomes $F_2 - F_3 + 2F_w = \rho Q(v_3 - v_2)$, which has been treated in Henderson (1966).

It is important to note that Eq. (3.14) assumes the pressure force on the block of water exerted by one sidewall of the expansion equal to that exerted by the other sidewall. This implies that the flow in the expansion is symmetric. Give $b_3/b_1 > 1.5$, asymmetric flow pattern is expected. The error introduced due to this approximation will be examined later.

By substitutions of Equations (3.9), (3.10) and (3.13) into Equation (3.14), and use of the relationship $L_2 \tan(\alpha/2) = 0.5(b_3 - b_2)$, the momentum equation may be rewritten as

$$\frac{1}{2}gb_2y_2^2 - \frac{1}{2}gb_3y_3^2 + \frac{1}{2}g(b_3 - b_2)\eta(\xi)^2 = Q(v_3 - v_2) \qquad (3.15)$$

The flow velocity terms can be replaced with the equation of continuity. The equation of continuity is given by

$$v_2 = \frac{Q}{b_2y_2} \qquad (3.16a)$$

$$v_3 = \frac{Q}{b_3y_3} \qquad (3.16b)$$

Substituting the flow velocities from Equations (3.16a,b) into Equation (3.15) will yield a cubic equation with real coefficients for the depth of flow, y_3, at the downstream end of the expansion.

3.8   Normalised Momentum Equation

If y_3 is scaled by the depth of the approaching flow, y_2, the dimensionless depth of flow $y_3^*(= y_3/y_2)$ is given by

$$y_3^{*3} + p_\circ y_3^* + q_\circ = 0 \qquad (3.17a)$$

with
$$p_\circ = \left(\frac{b_2}{b_3} - 1\right)\left[\frac{\eta(\xi)}{y_2}\right]^2 - \frac{b_2}{b_3} - \frac{2Q^2}{gb_2b_3y_2^3} \qquad (3.17b)$$

$$q_\circ = \frac{2Q^2}{gb_3^2y_2^3} \qquad (3.17c)$$

In fact, the flow before entering the expansion can be considered as uniform flow, and therefore y_2 is the same as y_1.

Let r denote the ratio of b_2 to b_3. This ratio is less than one for expansions. The expressions for p_o and q_o can be rewritten as

$$p_o = (r-1)\eta^{*2} - r(1 + 2Fr_2^2) \tag{3.18a}$$

$$q_o = 2r^2 Fr_2^2 \tag{3.18b}$$

with

$$\eta^* = \frac{\eta(\xi)}{y_2} \tag{3.18c}$$

η^* is equal to or greater than one. For approaching flow with the Froude number less than 0.70, p_o is negative.

Regarding the nature of the roots of the cubic equation (17a), three possible cases can be distinguished using the discriminate Q_o, defined as $Q_o = \left(\frac{p_o}{3}\right)^3 + \left(\frac{q_o}{2}\right)^2$ or

$$Q_o = \frac{1}{27}\left[(r-1)\eta^{*2} + r(2Fr_2^2 - 1)\right]^3 + r^4 Fr_2^4 \tag{3.19}$$

For subcritical flows with $Fr_2 \leq 0.7$ through expansions of relative large b_3/b_2 ratios, the determinant is less than zero. Equation (3.17a) has three possible roots, given by

$$y_3^* = 2\sqrt{-\frac{p_o}{3}} \cos\left(\frac{\beta_o}{3}\right) \tag{3.20a}$$

$$y_3^* = -2\sqrt{-\frac{p_o}{3}} \cos\left(\frac{\beta_o}{3} + 60°\right) \tag{3.20b}$$

$$y_3^* = -2\sqrt{-\frac{p_o}{3}} \cos\left(\frac{\beta_o}{3} - 60°\right) \tag{3.20c}$$

where $\cos\beta_o = -\dfrac{q_o}{2\sqrt{-(p_o/3)^3}}$. Equation (3.20a) gives positive values for the depth of flow at

CS 3 that is subcritical. Although Equation (3.20b) also produces positive solutions for some of

the approaching flow (with a depth up to $y_2 = 20$ cm, the solution being negative for $y_2 = 22$ cm), the resultant depth of flow at CS 3 is supercritical and therefore the solutions from this equation should be rejected. Equation (3.20c) gives negative values for the depth of flow, and thus is of no physical meaning. In summary, the solutions from Equation (3.20a) are acceptable and are presented in Table 3.2.

The corresponding flow velocity at the downstream cross section of the expansion or at CS 3 can be obtained from

$$v_3 = \frac{Q}{b_2 f(y_2, \eta, Q)} \tag{3.21}$$

Calculated flow velocity at CS 3 is needed for the evaluation of the velocity head as part of the specific energy at the cross section. The difference in specific energy between the upstream cross section CS 1 and the upstream cross section C3 will show the energy loss in the channel expansion.

3.9 Calculation of Energy Losses

The use of the energy and momentum concepts in a complementary manner allows the determination of the unknown energy loss in the energy equation. For a given flow depth y_1 and the Froude number Fr_1 at the upstream, Equations (3.20a,b,c) provide solutions of the flow depth y_3 at the downstream end of the expansion or at CS 3 (Figure 3.1). Substituting y_3 into Equation (3.5) allows the calculation of energy loss h_e. The upstream flow depth y_1 for this calculation is supplied from experimental measurements. Some sample calculations are shown in Table 3.3.

The most important results presented in Table 3.3 are the predicted depth of flow y_3 at CS 3 and the energy loss coefficient k_E. This energy loss coefficient is defined as

Table 3.2   Calculated depth of flow at CS 3 using the momentum concept. The depth ratio is given as $y_3* = y_3/y_1$. The calculations assume zero energy losses.

y_1 (cm)	10	12	14	16	18	20	22
Fr_1	0.59	0.45	0.35	0.29	0.24	0.21	0.18
			$\eta* = 1.01$				
q_o	0.242	0.140	0.088	0.059	0.042	0.030	0.023
p_o	-1.418	-1.243	-1.155	-1.105	-1.075	-1.056	-1.043
$\cos \beta_o$	-0.039	-0.019	-0.011	-0.007	-0.004	-0.003	-0.002
y_3*	1.094	1.054	1.034	1.023	1.017	1.013	1.010
			$\eta* = 1.02$				
q_o	0.242	0.140	0.088	0.059	0.042	0.030	0.023
p_o	-1.422	-1.248	-1.159	-1.109	-1.079	-1.060	-1.047
$\cos \beta_o$	-0.040	-0.019	-0.011	-0.007	-0.004	-0.003	-0.002
y_3*	1.100	1.060	1.040	1.030	1.023	1.019	1.016
			$\eta* = 1.03$				
q_o	0.242	0.140	0.088	0.059	0.042	0.030	0.023
p_o	-1.426	-1.252	-1.163	-1.113	-1.083	-1.064	-1.051
$\cos \beta_o$	-0.040	-0.019	-0.011	-0.007	-0.005	-0.003	-0.002
y_3*	1.104	1.064	1.045	1.034	1.027	1.023	1.021

$$k_E = \frac{H_1 - H_3}{v_1^2 / (2g)} \tag{3.22a}$$

where H_i is the total energy head equal to the sum of velocity head, elevation head and pressure head. The subscript $i = 1$ and 3 is used for the upstream cross section (CS 1) and for the downstream cross section (CS 3), respectively. In a horizontal channel, Equation (3.22a) becomes

$$k_E = \frac{E_1 - E_3}{v_1^2 / (2g)} \tag{3.22b}$$

Both y_3 and k_E appear to be sensitive to the dimensionless parameter η^*, given in Equation (3.18c). The former is also sensitive to the Froude number Fr_1 at the upstream cross section or

CS1, whereas the latter is somewhat so. Fr_1 ranges from 0.18 to 0.59 in the calculations (Table 3.3).

When η^* is given the lower limiting value or 1, the energy loss coefficient, k_E, is almost a constant value of 0.47. For $\eta^* = 1.01$, k_E ranges from 0.34 to 0.44, corresponding to Fr_1 equal to 0.18 and 59, respectively. The use of higher values for η^* can lead to unacceptable results of negative energy losses. In such a case calculations of the energy loss coefficient are omitted, indicated by the symbol '−'. The erroneous results are due to three possible reasons. The first possible reason is an estimation of the pressure force exerted by the sidewalls on the flowing water in the channel expansion. The second possible reason is that the two pressure forces on the sidewalls are not equal. The third reason is that the pressure on the sidewalls is non-hydrostatic. Notice that the results presented in Table 3.3 are based on the assumption of hydrostatic pressure distributions.

Table 3.3   Calculated depth of flow at CS 3 using the momentum concept and calculated energy losses, for a flat-bottom expansion. The depth ratio is given as y_3^* = y_3/y_1.

y_1 (cm)	10.00	12.00	14.00	16.00	18.00	20.00	22.00
E_1 (cm)	11.71	13.19	14.87	16.67	18.53	20.43	22.35
Fr_1	0.59	0.45	0.35	0.29	0.24	0.21	0.18
			$\eta^* = 1.00$				
y_3^*	1.092	1.052	1.032	1.0213	1.015	1.0108	1.0081
y_3 (cm)	10.92	12.62	14.45	16.34	18.27	20.22	22.18
v_3 (cm/s)	32.07	27.74	24.22	21.42	19.16	17.31	15.78
E_3	10.93	12.63	14.46	16.35	18.28	20.22	22.19
E_1-E_3	0.78	0.56	0.41	0.32	0.25	0.20	0.17
k_E	0.457	0.468	0.474	0.475	0.475	0.475	0.474
			$\eta^* = 1.01$				
y_3^*	1.09	1.05	1.03	1.02	1.02	1.01	1.01
y_3 (cm)	10.94	12.64	14.48	16.37	18.30	20.26	22.22
v_3 (cm/s)	32.00	27.68	24.18	21.37	19.12	17.28	15.75
E_3	10.95	12.66	14.49	16.39	18.31	20.27	22.23
E_1-E_3	0.762	0.532	0.385	0.284	0.215	0.162	0.122
k_E	0.445	0.447	0.440	0.425	0.407	0.378	0.344
			$\eta^* = 1.02$				
y_3^*	1.10	1.06	1.04	1.03	1.02	1.02	1.01
y_3 (cm)	10.96	12.67	14.51	16.41	18.34	20.30	22.27
v_3 (cm/s)	31.94	27.63	24.13	21.33	19.08	17.24	15.72
E_3	11.48	13.06	14.80	16.64	18.53	20.45	22.40
E_1-E_3	0.238	0.132	0.071	0.030	0.002	_	_
k_E	0.139	0.111	0.082	0.045	0.003	_	_
			$\eta^* = 1.03$				
y_3^*	1.10	1.06	1.04	1.03	1.02	1.02	1.01
y_3 (cm)	10.98	12.69	14.54	16.44	18.38	20.34	22.31
v_3 (cm/s)	31.88	27.57	24.08	21.29	19.04	17.21	15.68
E_3	11.50	13.08	14.83	16.67	18.56	20.49	22.44
E_1-E_3	0.219	0.108	0.043	_	_	_	_
k_E	0.127	0.091	0.049	_	_	_	_

Chapter Four   Experimental Setup and Experiments

4.1   Introduction

In this chapter, the experimental facility used in this study is described. Descriptions begin in Section 4.2 with a discussion on a re-circulating flume, the main component of the setup. The flume has been designed, assembled and installed in the Hydraulics Engineering Laboratory at Concordia University. One of the most important sections of the flume is an expansion, with or without bottom variations. The geometric features of the expansion are discussed in Section 4.3. The remaining sections of this chapter are devoted to measurement devices. A V-notch is used for flow measurements and a gate is installed at the downstream end of the channel for depth control. These are explained in Section 4.4. Section 4.5 discusses details about pressure taps connected to the sidewalls and the bottom of the expansion. In Section 4.6, point gauges used for measurements of the water surface are briefly introduced. Lastly in Section 4.7, the experimental procedures are explained.

4.2   Re-circulating Flume

The major component of the experimental facility for flow experiments is a re-circulating flume (Figure 4.1a), schematically shown in Figure 4.1b. The flume consists of multiple sections of channel as well as an expansion, which were made in the Machine Shop of the Department of Building, Civil and Environmental Engineering at Concordia University. These channel sections and expansions are installed in the Hydraulics Engineering Laboratory. The experimental setup is suitable for performing experiments based on the theoretical considerations discussed in

Chapter 3. During an experiment, the direction of the flow is from right to left, as indicated by an

arrow in the figure.

(a)
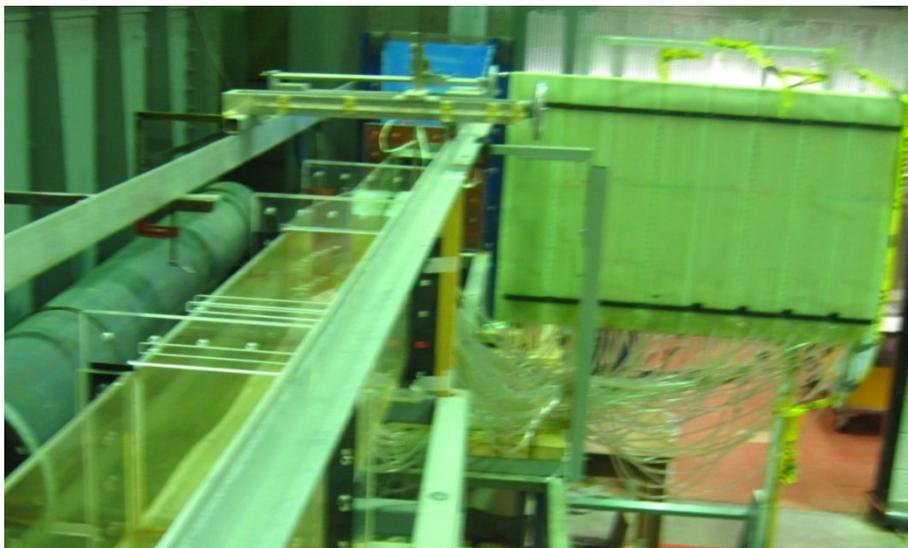
(b)
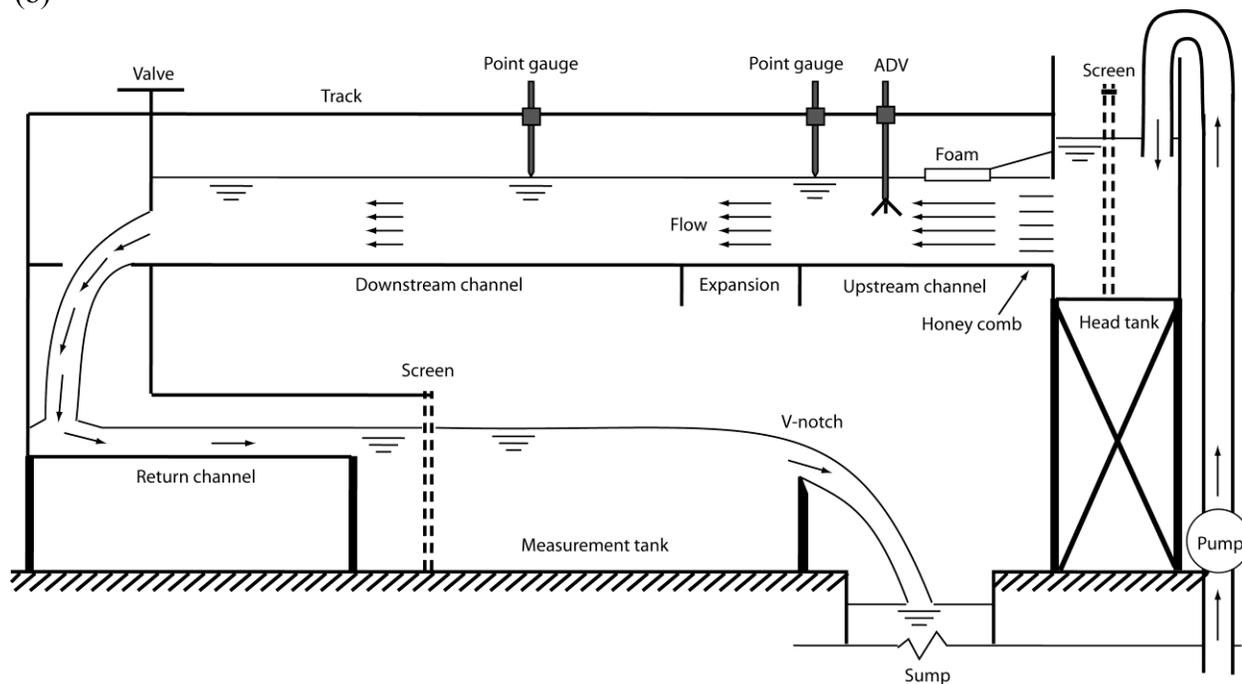
Figure 4.1   (a) Experimental setup used to conduct experiments in this study. (b) Schematic

illustrations of the upstream channel-section, the expansion and the downstream channel-section.

Measurement devices include point gauges, flow meters and a sharp-crested V-notch weir.

From upstream to downstream, the experimental setup consists of a pump, a head tank, an upstream channel-section, a channel expansion with or without a hump on the channel bottom, a downstream channel-section, a control gate at the downstream end of the flume, a measurement tank equipped with a 30° triangular or V-notch sharp-crested weir, and an underground sump. Pressure taps (1/16" diameter holes) are installed at the sidewalls in 4 rows and on the channel bottom of the expansion (Figure 4.2). The pump provides a steady flow rate. The head tank has a width of 4 ft, a length of 4 ft, and a height of 5 ft. A contraction (4:1) Immediately downstream of the head tank, a float is kept on the free surface to dampen surface waves. The channel sections as well as the expansion are built with smooth-surfaced plexiglasses and hence have a very low roughness height.

4.3 Expansion Section of the Channel

The channel expansion connects the upstream channel-section with the downstream channel-section, as shown in Figure 3.1. These three components rest on the level top of a supporting metal frame, which elevates the channel bottom 150 cm above the laboratory floor (Figures 4.1a,b). The configuration of the whole channel is shown in Figure 3.1, and the dimensions of the various components are listed in Table 4.1. The ratio of L_1 to L_2 is close to 4, whereas the ratio of L_3 to L_2 is larger than 13. So the transition is considered to be short. Along the expansion's longitudinal length of 32.33 cm, the flume increases linearly in width by 11.09 cm; the corresponding expansion angle is $\alpha = 19.46°$ (Figure 3.1). The sidewalls of the flume are 30.48 cm high. All the experiments allowed a free board of at least 5 cm for safety reasons.

The expansion is considered as a gradual expansion, with $0.5(b_3 - b_1)/L_2 < 0.25$, which is the 1:4 taper normally recommended for the design of an expansion (Henderson 1966),

optimised to reduce energy head loss due to an expansion. Nevertheless, since $b_3/b_1 = 1.667$ (> 1.5), the expansion used in this study is expected to be more influential to the total energy loss than the condition (the Froude number) of the upstream flow, as is the case for an abrupt expansion.

Table 4.1   Geometric characteristics of the expansion used in this study.

Geometric parameter	Value
Upstream channel section width (b_1)	171.1 mm
Downstream channel section width (b_3)	289.3 mm
Upstream channel section length (L_1)	1235.4 mm
Channel expansion length (L_2)	323.3 mm
Downstream channel section length (L_3)	4403.5 mm
Rate of sidewall flare [$1:(b_3-b_1)/2L_2$]	1:0.183
Width ratio ($r = b_3/b_1$)	1.69
Central angle between sidewalls (α degree)	18°4'
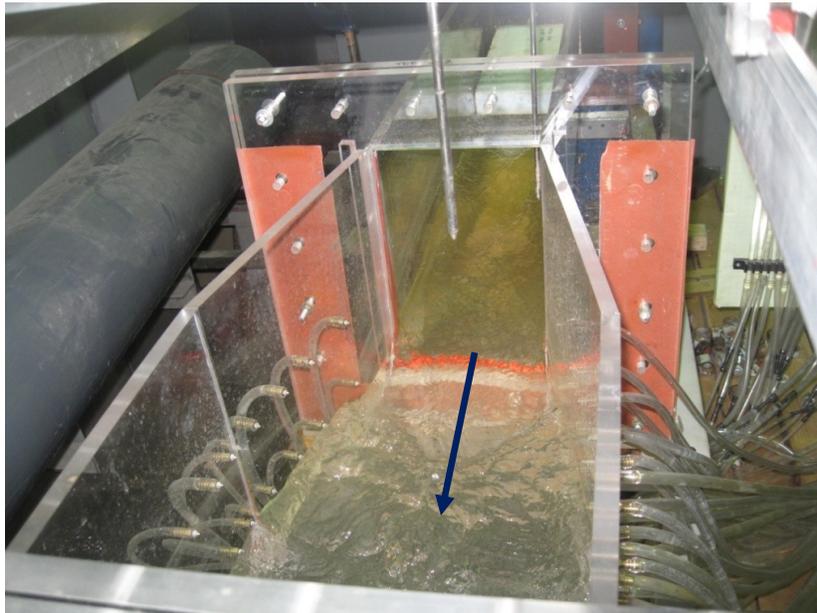
Figure 4.2   Channel expansion and 1/16" wall pressure taps through the wall and connected to piezometers. This photo shows the expansion with a hump fitted on the channel bottom.

In pipe flow experiments, Mehta (1979) reported that flows in two-dimensional sudden expansions are asymmetric and unstable, with three-dimensional character when the expansion ratio is larger than 1.25. In this study, the ratio is 1.668.

On the other hand, the channel expansion is not long (323.3 mm in length), relative to its width (285.2 mm at the downstream end) and relative to the depth of flow (up to 250 mm in the experiments reported in this study). Thus, the expansion is not expected to cause a significant frictional loss of energy head, compared to that caused by potential flow separation.

Experiments were performed using both the channel expansion with a flat bottom and the expansion with a hump on the channel bottom in order to make comparisons of respective experimental results. The hump fitted on the channel bottom is shown in Figure 3.4. The design of the hump is as follows. Beginning at its upstream end, the channel expansion has an adverse bottom-slope of slightly less than $S = 2\%$, which is steep compared to typical slopes in natural river channels. The channel bottom is raised linearly, by 0.635 cm at the downstream end of the expansion, and then drops linearly, with a favourable slope equal to S, down to the bottom level at the upstream end of the expansion. Thus, variations in the channel bottom are symmetric about the downstream end of the channel expansion.

It is important to note that changes to the stage of flow (including flow depth and flow velocity) due to the transition may persist over a long distance downstream of the transition, although the transition itself is short.

4.4   Discharge and Depth Controls

Water is pumped up from the underground sump to the head tank at desired flow rates. A honey comb is fitted into the outlet of the head tank leading into the upstream channel-section.

Immediately downstream of the honey comb, a floating foam is held on the water surface. Such a configuration helps dampen surface waves that disturb the flow through the flume; ideally the flow is to be maintained as steady.

For a given total discharge, to control the depth of flow through the flume and hence the Froude number of the flow, the downstream control gate is set to fully or partially open (Figure 4.3). This control provides desired values for the Froude number.

A return channel downstream of the control valve leads water to the measurement tank. This tank has a width of 90.17 cm. The sharp-crested V-notch weir installed at the downstream end of the tank is fully contracted (Figure 4.3). The height of the crest is $P = 58.00$ cm above the bottom of the tank, much larger than the recommended minimum height of 9 cm (Kindsvater and Carter 1957). Heads for calculating the total discharge through the V-notch weir were measured at a distance of 143.00 cm upstream of the weir. This distance is more than four times the maximum actual head intended in the experiments. During the experiments, the free flowing nappe through the V-notch returned water back to the sump. The underside of the nappe was at atmospheric pressure. The expected maximum error for discharge measurements is 3%. The depth measurements were made to the nearest 0.1 mm.

For the experiments, heads in the measurement tank above the crest of the V-notch weir were in the range of 6 to 23 cm. The lower limit was maintained in order to avoid potential measurement error at such small heads and to avoid the nappe clinging to the weir, which affects the accuracy of the head-discharge relationship. The upper limit was maintained to satisfy $H / P \leq 0.4$, which is one of the conditions for the V-notch weir to remain fully contracted. For fully contracted V-notch weirs, values for the coefficient of discharge and the head correction factor are a function of the notch angle only (Bos 1989); the use of these values is of certainty.

Figure 4.3   The downstream gate used in the laboratory for depth and Froude number control.
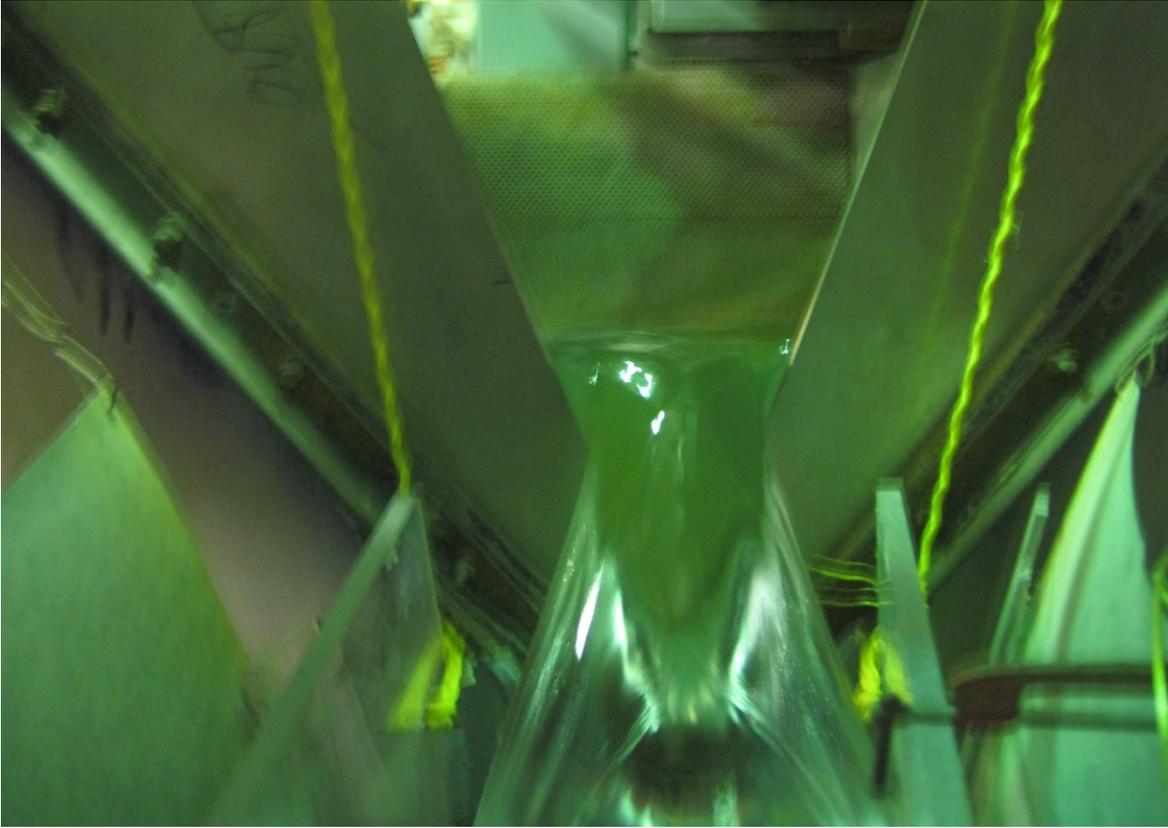
Figure 4.4   The 30° V-notch weir used in the laboratory for discharge measurements.

The total discharge is obtained from measurements of heads above the crest of the V-notch, using the following head-discharge relationship

$$Q = C_d \frac{8}{15} \sqrt{2g} \tan\left(\frac{\theta}{2}\right)(H + k_h)^{5/2}$$

(4.1)

where Q is the total discharge (m^3/s), C_d is the coefficient of discharge, θ is the notch angle in degree, H is the head measured above the weir crest (m), and k_h is the head correction factor (m). The values of C_d and k_h are taken as 0.585 and 0.002 m, respectively. The precision of head measurements is 1 mm, which translates into discharge precision of 1.17×10^{-5} L/s through Equation (4.1).

It is difficult to directly access the v-notch. Therefore, a connected tube is set up so that reading of the water level can easily be made. A velocity meter is available for two reasons. First, it provides direct measurements of instantaneous flow velocities distributed at cross sections upstream and downstream of the channel expansion. Secondly, together with the measurements of flow depth from point gauges and cross-sectional areas, the flow velocity measurements allow calculations of the total discharge in order to confirm the V-notch measurements.

4.5   Pressure Taps

An array of distributed pressure taps are installed on the sidewalls of the channel expansion (Figure 4.2). A series of evenly spaced pressure taps are also installed on the bottom of the channel expansion. The positions of the pressure taps are listed in Table 4.2. These positions are given on the Cartesian coordinates system that follows the right hand rule. The x-axis is placed horizontally along the middle of the flume, and points positively towards downstream (Figure 3.1); the y-axis is placed through the upstream end of the channel expansion or CS 2, in the cross-channel direction; and the z-axis points positively upwards, and z is equal to zero on the channel bed at CS 2.

Simple piezometers are connected to the pressure taps of 2 mm in diameter to provide pressure measurements. In the channel expansion with a flat bottom, there are 40 pressure taps on one of the sidewalls and 10 on the channel bottom. In the channel expansion with a hump fitted on the channel bottom, there are 40 pressure taps on each of the two sidewalls and 10 on the channel bottom.

Table 4.2   Positions of the pressure taps on the Cartesian coordinates system. The reference level or vertical datum is where z is equal to zero. There is a difference of 2 mm in channel-bed elevation between CS 2 and CS 3 (Figure 3.4).

pressure tap	x(mm)	y(mm)	z(mm)	pressure tap	x(mm)	y(mm)	z(mm)
A1	88.90	-102.75	152.11	D1	88.90	-102.75	12.41
A2	165.10	-117.54	151.86	D2	165.10	-117.54	12.16
A3	215.90	-127.40	151.69	D3	215.90	-127.40	11.99
A4	266.70	-137.26	151.53	D4	266.70	-137.26	11.83
A5	298.45	-143.42	151.42	D5	298.45	-143.42	11.72
A6	311.15	-144.65	151.38	D6	311.15	-144.65	11.68
A7	342.90	-144.65	151.28	D7	342.90	-144.65	11.58
A8	393.70	-144.65	151.11	D8	393.70	-144.65	11.41
A9	444.50	-144.65	150.94	D9	444.50	-144.65	11.24
A10	520.70	-144.65	150.69	D10	520.70	-144.65	10.99
B1	88.90	-102.75	75.91	Z1	88.90	-30.00	-0.29
B2	165.10	-117.54	75.66	Z2	165.10	-30.00	-0.54
B3	215.90	-127.40	75.49	Z3	215.90	-30.00	-0.71
B4	266.70	-137.26	75.33	Z4	266.70	-30.00	-0.88
B5	298.45	-143.42	75.22	Z5	298.45	-30.00	-0.98
B6	311.15	-144.65	75.18	Z6	311.15	-30.00	-1.02
B7	342.90	-144.65	75.08	Z7	342.90	-30.00	-1.13
B8	393.70	-144.65	74.91	Z8	393.70	-30.00	-1.29
B9	444.50	-144.65	74.74	Z9	444.50	-30.00	-1.46
B10	520.70	-144.65	74.49	Z10	520.70	-30.00	-1.71
C1	88.90	-102.75	25.11				
C2	165.10	-117.54	24.86				
C3	215.90	-127.40	24.69				
C4	266.70	-137.26	24.53				
C5	298.45	-143.42	24.42				
C6	311.15	-144.65	24.38				
C7	342.90	-144.65	24.28				
C8	393.70	-144.65	24.11				
C9	444.50	-144.65	23.94				
C10	520.70	-144.65	23.69				

The principle by which the piezometers work can be found in standard hydraulics textbooks. Water pressure has no variation normal to straight streamlines. Therefore, it is possible to measure the pressure of water using a wall pressure "tap", placed in a region where flow streamlines are straight. The pressure tap should be a small hole with the axis locally perpendicular to the surface (sidewall or channel-bed). The hole is made to be perpendicular to the channel and free of burrs. By connecting the tap to a piezometer it is possible to make accurate measurements of pressure in the flowing water.

4.6   Point Gauges

Along the length of the flume between the head tank at upstream and the control gate at downstream, several point gauges (Figure 4.2) are mounted along a pair of parallel tracks over the top of the flume (Figures 4.1a,b). These point gauges allow measurements of water surface elevation at selected locations. The accuracy of the point gauges is within 0.1 mm. It is important to note that the presence of water surface waves makes it difficult to obtain such accuracy. To alleviate the spatial fluctuations due to the surface waves (Figure 3.2), measurements are made at three to five more or less evenly spaced locations across the width of the channel. The average of the multiple point measurements is more representative for the cross section of interest than the measurement at individual locations.

4.7   Experimental Procedures

The experimental procedures for measurements are summarised as follows:

a. Maintain a steady pumping rate.

b. Record the initial and final water surface elevations of the V-notch weir.

c. Determine the total discharge through the V-notch.

d. Verify the calculated total discharge using the volumetric method.

e. Measure the water surface elevation of the approaching flow at three or more locations across the width of the channel.

f. Calculate the cross-sectional mean velocity of the approaching flow.

g. Repeat steps (e) and (f) for the downstream flow at the downstream end of the expansion.

h. Record the expansion bottom pressures distributed along the length of the expansion.

i. Record the sidewall pressures distributed along the length of the expansion and at different heights above the expansion bottom.

Chapter Five   Results   for   Experiments   with   a   Flat-bottom Expansion

5.1   Introduction

This chapter begins in Section 5.2 with the verification of discharges for flow experiments with a flat-bottom expansion. The conditions of the flows that approach the expansion are described in Section 5.3. The Froude number is evaluated so as to confirm the condition of subcritical flow. Also, the Reynolds number is evaluated to justify the omission of viscous forces in the momentum concept discussed in Chapter 3. Section 5.4 presents the experimental and theoretical results about the coefficient of energy loss in the expansion.

The remaining sections deal with variations in water pressure. An adverse pressure gradient or increasing pressure in the direction of the flow often triggers flow separation. Experimental evidences of an adverse pressure gradient in the expansion are shown in Section 5.5 over the entire water column and in Section 5.6 along the water surface. The vertical variations in pressure are examined in Section 5.7. What is particularly interesting is to reveal if the hydrostatic distribution is adequate to describe the pressure variations in the vertical. Finally, the pressure forces on the expansion sidewall for the experiments are evaluated in Section 5.8.

5.2   Discharge Verification

Discharges or flow rates are regulated by a control valve of the pumping system (Figure 4.1b). During an experiment the pumping of water from the sump is kept at a steady rate. The head over the crest of the sharp-crested V-notch weir (Figure 4.4) is measured, and from this measured head the discharge in the re-circulating flume (Figures 4.1a,b) is calculated using Equation (4.1), denoted by Q_{vn}. A set of seven different V-notch discharges are shown in Figure

5.1. Although sharp-crested weirs are known to produce discharge measurements close to their 'true values' with only small errors of as low as 3%, it is desirous to understand the certainty of the V-notch measurements.

For this purpose, the simple volumetric method is used to obtain an independent set of discharge measurements. This method involves collecting 10 litres or so of water from the nappe passing over the weir crest, and registering the elapsed time for the collection. The actual volume of the collected water is measured using a graduated cylinder. The ratio of the actual volume to the elapsed time gives the discharge. These procedures are repeated three times for a steady pumping rate. The average, denoted by Q_{vm}, of the three discharges is used for comparison with the corresponding V-notch measurement, as shown in Figure 5.1.
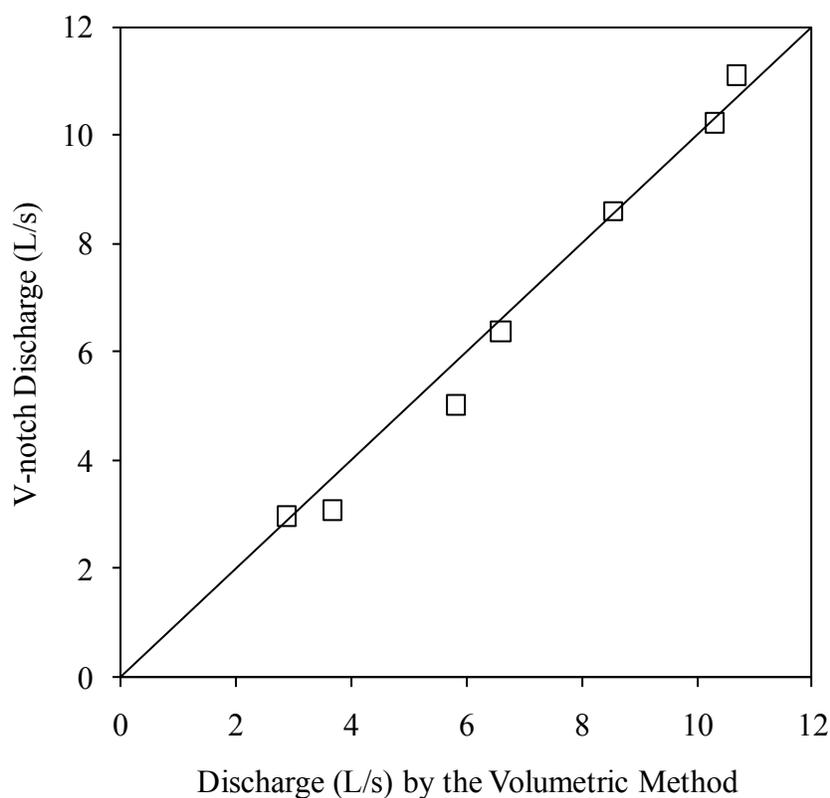
Figure 5.1   Correlation of discharge measurements using the V-notch weir and the volumetric method.

In order to show how close the discharge measurements based on the two different methods are to each other, the correlation coefficient of the two data sets is calculated. The equation for the correlation coefficient is

$$Correl(Q_{vn},Q_{vm}) = \frac{\sum(Q_{vn}-\overline{Q}_{vn})(Q_{vm}-\overline{Q}_{vm})}{\sqrt{\sum(Q_{vn}-\overline{Q}_{vn})^2\sum(Q_{vm}-\overline{Q}_{vm})^2}} \qquad (5.1)$$

where $\overline{Q}_{vm}$ is the average of discharges by the volumetric method, and $\overline{Q}_{vn}$ is the average of the V-notch discharges. The correlation coefficient of the two data sets shown in Figure 5.1 is 0.994. Thus, both the V-notch weir and the volumetric method have produced statistically the same discharge measurements. In fact, the differences between the corresponding discharge measurements from the two methods have a mean value of 0.21 L/s and a standard deviation of 0.29 L/s. These results of the mean value and standard deviation are very small, compared to $\overline{Q}_{vn}$ of 6.77 L/s. Subsequently, the V-notch measurements, hereafter denoted by Q, are used.

5.3   Experimental Conditions of the Upstream Flow

A total of six experiments (Table 5.1) were conducted with a flat-bottom expansion where the channel bed was flat. The discharge ranges from Q = 8.59 to 11.11 L/s, giving an average of 10.25 L/s. The discharges are obtained from Equation (4.1), where the head H is the difference between observed final water-surface elevation y_f and the initial water-surface elevation y_i (above an arbitrary datum) in the measurement tank (Figure 4.1b and Figure 4.4). The initial water-surface elevation is measured when the water surface just reaches the crest of the V-notch.

The upstream flow depth y_1 is taken as the difference between the initial point-gauge reading (bottom of the channel) and final point-gauge reading (water surface), shown in Figure 4.2. The precision of the point gauge is 0.1 mm. The upstream flow depth ranges from 11.12 to 18.57

(cm), with an average of 15.20 (cm). The upstream flow depth has been controlled with the downstream gate (Figure 4.3).

Table 5.1 A summary of experiments with a flat bottom expansion. The water temperature was T = 22.5°C. The independent variable is the dimensionless Froude number.

Experiment	Q (L/s)	y_1 (cm)	v_1 (cm/s)	Fr_1	Re
E11	10.23	18.57	32.21	0.24	18856
E12	10.23	17.45	34.27	0.26	19666
E13	10.23	15.44	38.73	0.31	21313
E14	11.11	14.87	43.69	0.36	23716
E15	11.11	13.77	47.17	0.41	24881
E16	8.59	11.12	45.21	0.43	21850

The flows in all the experiments listed in Table 5.1 are subcritical, as the Froude number, given in Equation (3.4), has values of less than unity. An attempt has been made to conduct experiments with higher values for the Froude number. However, the presence of large-amplitude (larger than 2 mm by visual examination) surface waves have created a significant uncertainty in measurements of the depth of flow in the expansion, and therefore, the experimental results are not reported in this study.

For the purpose of evaluating the Froude number as well as the velocity head, the flow velocity at the upstream is calculated as the ratio of the V-notch discharge to the cross sectional area. The cross sectional area is simply the upstream channel width multiplied by the flow depth from point gauges. As discussed in Chapter 4, in order to smooth out disturbing surface waves, which have appeared in some of the experiments with relatively high Froude number, point

gauge measurements have been obtained at up to six points across the channel. The average of these measurements gives the flow velocity shown in Table 5.1. It is understood that the flow velocity varies from point to point at any given channel cross section.

The experiments listed in Table 5.1 have high values for the Reynolds number, defined as

$$\mathrm{Re} = \frac{\rho v_1 R_h}{\mu} \tag{5.2}$$

where R_h is the hydraulic radius, and μ is the dynamic viscosity of water, being dependent of water temperature. Since the Reynolds number is as high as around 2.0×10^4, the flows are fully turbulent in all the experiments. This common feature of the flows justifies the omission of viscous forces in the momentum equation (3.14).

5.4   Coefficient of Energy Loss

The energy losses have been calculated for both the experiments and predicted flow conditions. The predictions assume reason Froude number values with different η^* (Table 3.3). The energy loss in the expansion is found by subtracting the specific energy at the downstream end of the expansion or at CS 3 from the specific energy at the upstream cross section or at CS 1 (Figure 3.1). Then, the energy loss coefficient k_E is determined by dividing the energy loss by the velocity head at CS 1. The mathematical expression is given in Equation (3.22b). Notice that the expansion which is used is a gradual expansion.

The k_E values for the six experiments, listed in Table 5.1, are plotted in Figure 5.2. The two dashed curves are based on predicted depth of flow at Figure 5.2, for two different values of η^*. The experimental results show k_E values in the range of 0.4 to 0.6. The theory gives k_E values in good agreement with the experimental results for the Froude number larger than 0.3. At

lower Froude number values, the theoretical k_E values are also close to the experimental data. It would be interesting to compare the results from this study to the energy loss coefficient given in Henderson (1996, p.236) for a sudden expansion.
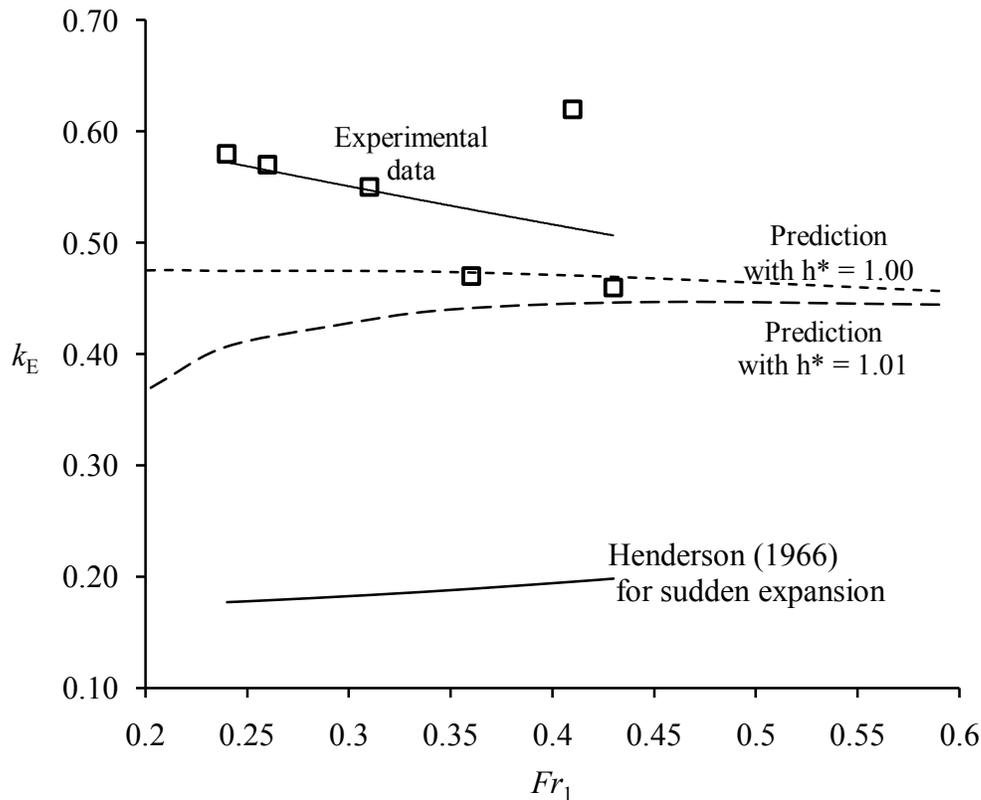
Figure 5.2   Comparisons of the coefficient of energy head loss between experiments and theoretical predictions. In the experiments the Froude number ranges from 0.24 to 0.43, and the coefficient is between 0.46 and 0.62. The dependence of k_E on the Froude number appears to be weak.

In the limiting case of $\alpha = 180°$, the channel transition becomes a sudden expansion (Figure 3.1). Henderson (1966, p. 236) presented an equation for determining the energy loss, given by

$$E_1 - E_3 = k_E \frac{v_1^2}{2g} \tag{5.3}$$

with the coefficient of energy loss given by

$$k_E = \left(1 - \frac{b_1}{b_3}\right)^2 + \frac{2Fr_1^2 b_1^3 (b_3 - b_1)}{b_3^4} \tag{5.4}$$

The first term on the right hand side of the above expression represents the contribution from the changing width of the expansion to the total energy head loss. For the specification of expansion given in Table 4.1, the first term is equal to 0.167. The second term involves both the effect of the changing width and the Froude number of the flow. According to Henderson (1966), the second term does not contribute significantly to the total energy head loss unless $Fr_1 > 0.5$ or $b_1/b_3 > 0.66$; since both conditions are not satisfied for the experiments conducted in this study, the second term is not significant.

The k_E value determined from Equation (5.4) is for a sudden expansion and therefore should be higher than the k_E value given by Equation (3.22b) for the gradual expansion with the same width ratio, but it is not. As shown in Figure 5.2, the k_E values determined from Equation (5.4) using b_1 and b_3 values from Table 3.1 and the Froude number from Table 5.1 are plotted below the experimental results and predictions of this study using the momentum concept combined with the energy concept, as discussed in Chapter 3. A possible explanation is that the restriction that Fr_1 is small enough for Fr_1^4 and higher powers to be neglected, needed to derive Equations (5.3) and (5.4), is not valid in this study.

5.5   Adverse Pressure Gradient

The phenomenon of flow separation from a solid boundary has been discussed extensively in many standard textbooks (e.g. White, 2006). The formation of turbulent eddies in the separation zone can cause significant energy dissipation in the flow. Detailed discussion on the phenomenon and associated energy dissipation is beyond the scope of this study. This section limits the discussion to adverse pressure gradient, known as one of the factors that cause flow separation. The pressure taps whose positions are listed in Table 4.2 produce measurements for determining the gradient of water pressure in the direction of flow.

In Figure 5.3, the expansion's upstream end is located at $x = 0$, and its downstream end is marked by the dotted vertical line at $x = 304.8$ mm. The dotted horizontal line drawn through the symbol o is the channel bottom, and the solid line above the sidewall pressure taps is the water surface for experiment E11 (one of the experiments listed in Table 5.1), meaning that the pressure taps are submerged. The pressure taps from right to left on the top row are denoted by A1, A2, ..., A10. The pressure taps from right to left on the second row from the top are denoted by B1, B2, ..., B10. The pressure taps from right to left on the bottom row are denoted by Z1, Z2, ..., Z10. For complete details, refer to Table 4.2. Examples of water pressure varying in the horizontal direction are shown in Figures 5.4a-c.

Along horizontal lines through each row of pressure taps (Figure 5.3), the elevation is the same. In Figures 5.4a-c, only the five pressure taps in the expansion are shown. As expected, the pressure taps (Z1 throughout Z5) at the channel bottom record the highest water pressure, followed by pressure taps D1 to D5, C1 to C5, B1 to B5, and A1 to A5. The longitudinal variations in water pressure for each row of pressure taps show almost the same pattern. The pressure increases with increasing distance from the entrance of the expansion. In experiment E14, the top row of pressure taps is submerged just below the free water surface.
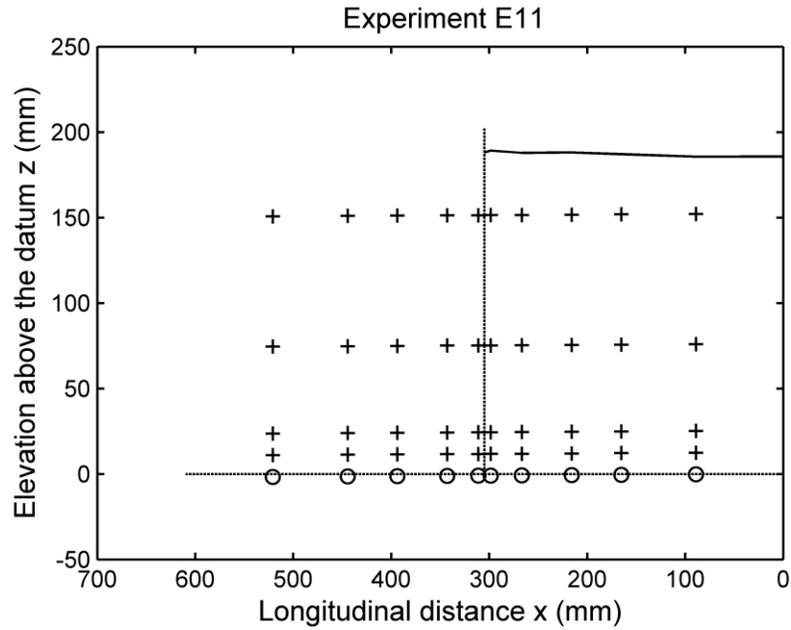
Figure 5.3   Positions of pressure taps drilled through the sidewall (marked by the symbol +) of the expansion and at the channel bottom (marked by the symbol ○). The flow is from right to left.

(a)
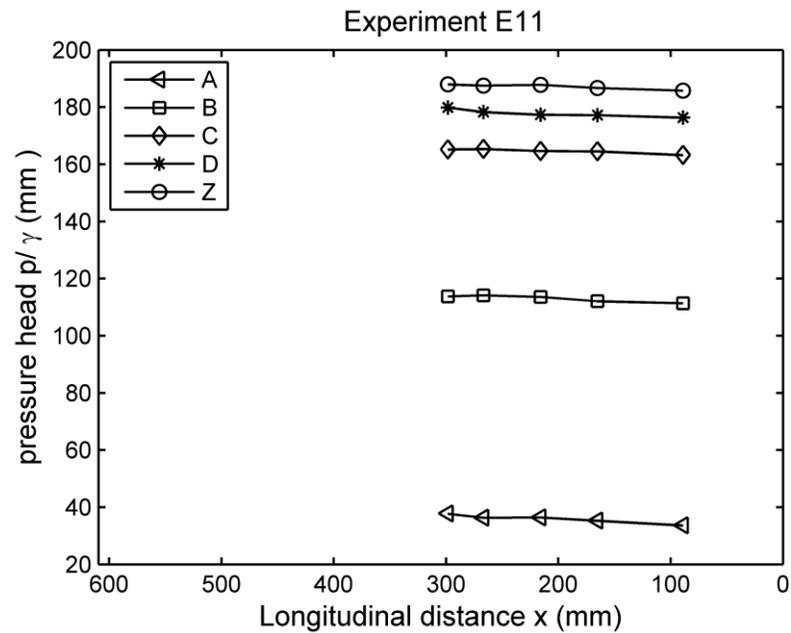
(b)
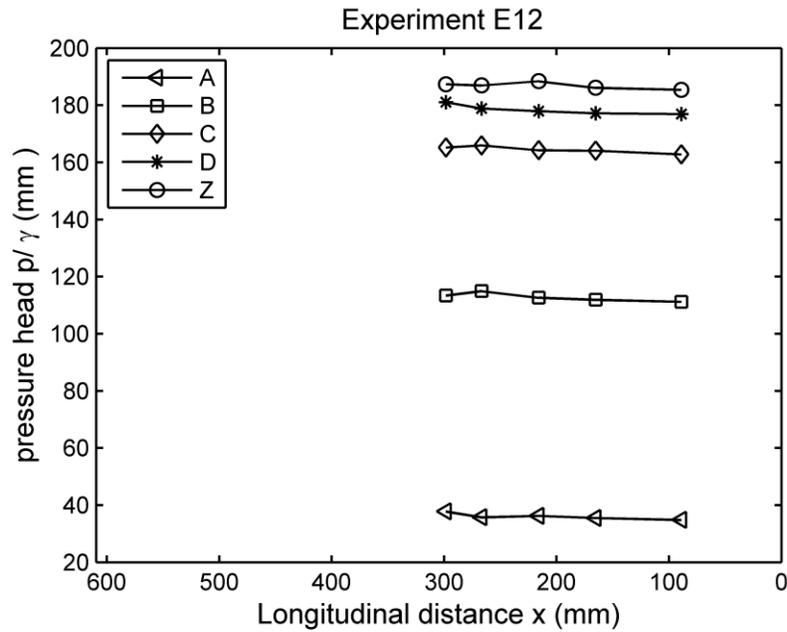
(c)
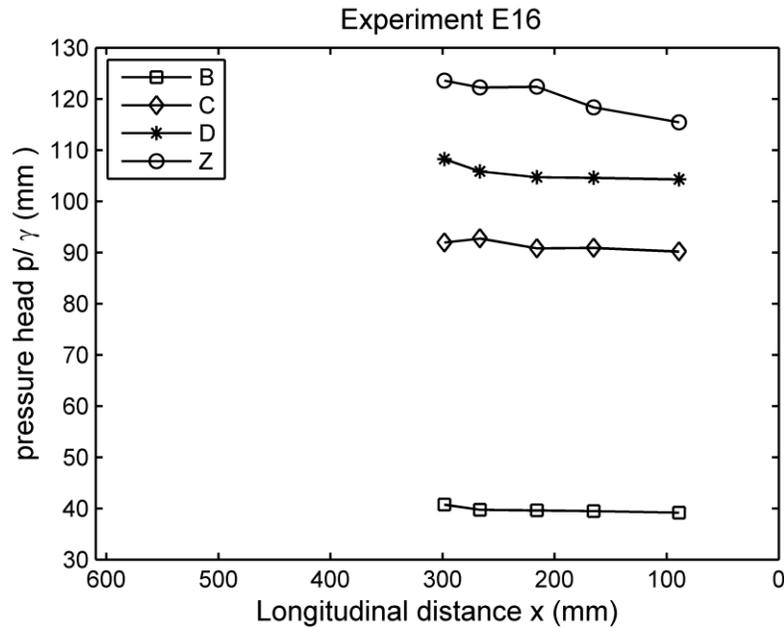
Figure 5.4   Longitudinal variations in pressure head shown for selected experiments. The flow is from right to left. The conditions of the experiments are listed in Table 5.1. The upstream and downstream ends of the expansion are located at $x = 0$ and 304.8 mm, respectively. A sudden increase in pressure head is possibly due to eddy motion.

Table 5.2 The strongest adverse pressure gradient, $\dfrac{1}{\gamma}\left(\dfrac{dp}{dx}\right)_{max}$, for different rows

of pressure taps for the experiments with a flat-bottom expansion.

Experiment	Maximum pressure gradient				
	A1–A5	B1–B5	C1–C5	D1–D5	Z1–Z5
E11	0.044	0.030	0.017	0.051	0.013
E12	0.063	0.046	0.034	0.069	0.046
E13	0.051	0.038	0.034	0.063	0.054
E14	0.082	0.012	0.018	0.038	0.046
E15	–	0.022	0.030	0.082	0.038
E16	–	0.032	0.038	0.022	0.050

In the longitudinal direction the dimensionless pressure gradient is defined as $\dfrac{1}{\gamma}\dfrac{dp}{dx}$, whose value

is expected to change from point to point. The maximum values for different rows of pressure

taps within the flat-bottom expansion for the six experiments are shown in Table 5.2. In

experiments E15 and E16 the water surface is below the top row of pressure taps (denoted by A1

to A5), and therefore no evaluations are done (shown by the symbol –). The table shows that in

all the experiments except E14 and E16, the bottom row of the sidewall, which is denoted by

D1–D5, has the largest pressure gradient for the same experiment. In experiments E14 and E16

the top row of pressure taps (A1–A5) and the pressure tap on the channel bottom (Z1–Z5) have

the largest value among all the rows, respectively.

By comparing the same row of pressure taps in all the experiments, it is found that

experiment E14 has produced the largest pressure gradient that occurred in the top row of

pressure taps (A1–A5). For the second row (from the top) of pressure taps (B1–B5), experiment

E12 has given the largest pressure gradient of all the experiments. Experiment E16 has yielded

the largest value for the largest pressure gradient for the third row of pressure taps (C1–C5). The largest value for the maximum pressure gradient for the fourth row of pressure taps (D1–D5) has been obtained in experiment E15. Finally, for the bottom pressure taps (Z1–Z5), the largest value for the maximum pressure gradient has been seen in experiment E16.

For all the experiments, of all the sidewall pressure taps, the global maximum pressure gradient has occurred in the top row of pressure taps in experiment E14. The same global maximum has been observed in the bottom row of the sidewall pressure taps (D1–D5) of the experiment E16. The global maximum value is 0.082. The above-mentioned results are summarised in Table 5.2. Overall, the adverse pressure gradient has been shown to be quite significant, and certainly has decelerated the flow.

5.6   Water surface profiles

Water surface profiles in the expansion are shown for two of the experiments listed in Table 5.1. In Figures 5.5a,b the dotted horizontal line is the channel bottom and the solid curve above all the pressure taps is the water surface profile. Notice that the flow becomes progressively shallower in a sequential order of experiments E11, E12, ..., E16. In other words, among these experiments, experiment E11 had the deepest flow, whereas experiment E16 had the shallowest. In fact, in experiments E15 and E16 the top row of pressure taps was unsubmerged, and in experiment E14 the water surface just matched the elevation of the top row of pressure taps.

The average slope of the water surface is calculated by dividing the difference in water surface elevation between the upstream and downstream ends of the expansion to the expansion length that is 304.8 mm. The average slopes of the water surface for experiments E11–E16 with the flat-bottom expansion is 0.0079, 0.0083, 0.0093, 0.0129, 0.0082, and 0.0140, respectively.

(a)

(b)
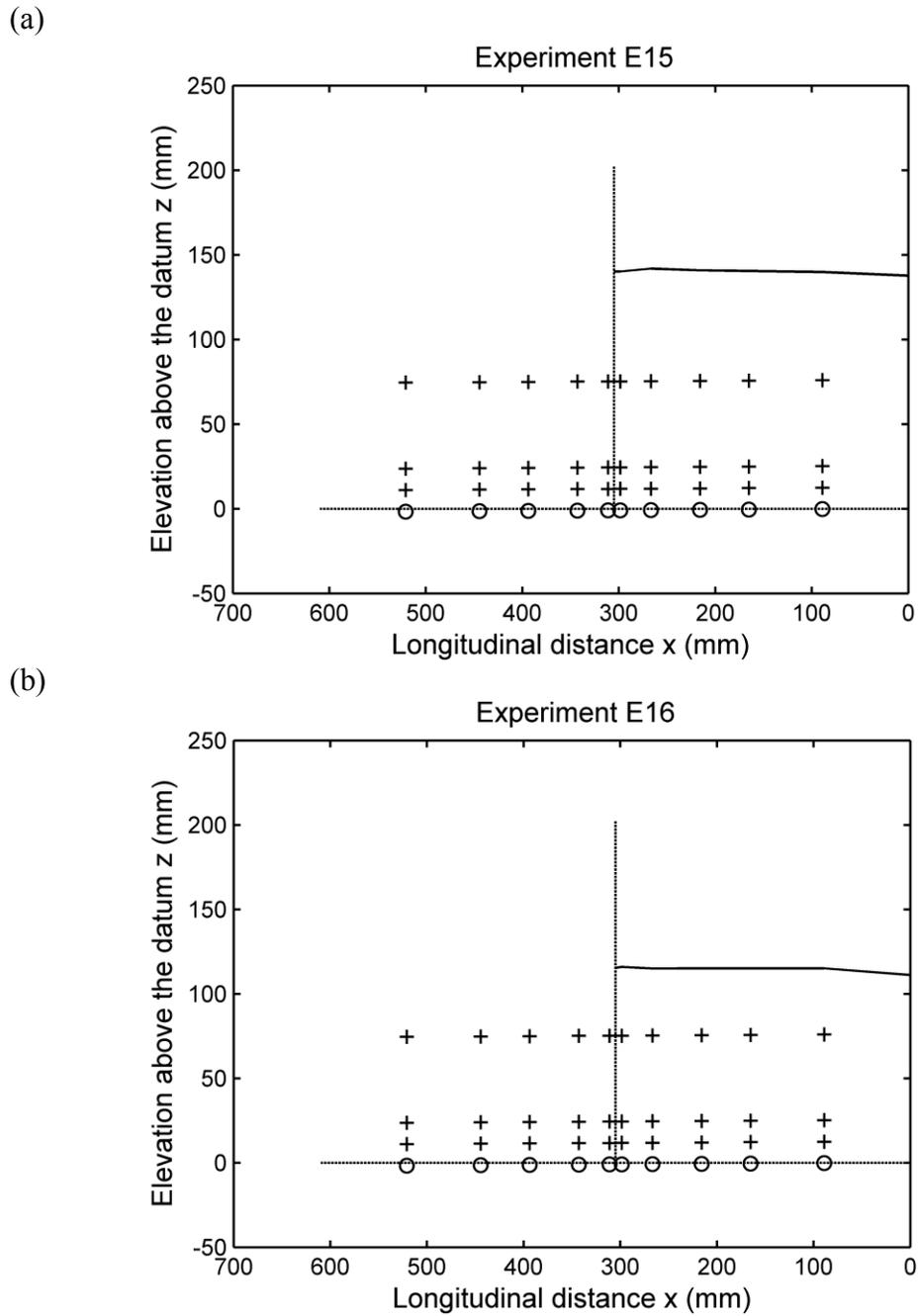
Figure 5.5   Water surface profiles shown as the solid curves above

the pressure taps. The sidewall pressure taps are marked by the symbol

+, and the bottom pressure taps are indicated by the symbol o.

These values show an interesting trend that the average slope increases from experiments E11 to

E16, with the exception of experiment E15 (From the experimental data, it is not clear what the

reason is). Thus, E16 has the maximum water surface slope and E11 has the minimum slope. It is possible that the increase in the slope of water surface is related to the increasing value for the Froude number from experiment E11 to E16 (Table 5.1).

Although the individual experiments have produced different water-surface slopes, all of them are positive values. This means that the water surface consistently titles up through the expansion from its upstream end. The positive water-surface slopes of the experiments are about 1%, which is large relative to the magnitude of typical negative slopes of natural river channels. It can be concluded that the positive water-surface slope in the expansion has a substantial impact on decelerating the flow. Positive water-surface slopes and adverse pressure gradients would have the effects of triggering flow separation from the expansion sidewall and hence dissipating flow energy.

5.7   Vertical distribution of water pressure

Knowledge of pressure distribution in the vertical is needed for the determination of pressure forces in the momentum equation. The flows in the experiments have been shown to be turbulent as the Reynolds number has values as high as 20000. As a result, the pressure distribution in the vertical would be at least locally non-hydrostatic, particularly near the sidewalls of the expansion. Here, the basic idea is to show to what extent the actual pressure can be approximated by the hydrostatic pressure distribution, which will simplify the calculation of pressure forces. The equation for the hydrostatic pressure distribution is

$$p_h = \gamma h \tag{5.5}$$

where γ is the specific weight, and h is the vertical distance between the water surface and the point of interest.

In Figures 5.6a-c, water pressures measured at the depths of pressure taps below the water surface are plotted for experiments E11, E13 and E15, respectively. For each of the three experiments, only the pressure taps A1– Z1, A2–Z 2 and A3–Z3 are included in the plots, as A4–Z4 and A5–Z5 show similar features. As shown in Figure 5.6a, the pressures for experiment E11 exhibits a linear relationship with depth over the entire water column. This is to say that the pressure distribution in the vertical is almost hydrostatic. The hydrostatic pressure distribution is also true for experiments E13 and E15, over a large portion of the water column, except near the channel bottom. Near the bottom the measured pressure deviated from hydrostatic pressure, being lower in Figure 5.6b (for E13), given by Equation (5.5), whereas higher in Figure 5.6c (for E15).

Let Δp be the deviation of the measured pressure, p, from the hydrostatic pressure, p_h, calculated from Equation (5.5). The deviation is given by

$$\Delta p = p - p_h$$

(5.6)

For all the experiments (Table 5.1) the deviations are almost zero over a large portion of the water column. The average of the largest deviation Δp for each of the six experiments has a lower and an upper limit of ± 40 N/m^2. The pressure deviations relative to the corresponding hydrostatic pressures are all less than 10%, as shown in Figures 5.7a-c Thus, the hydrostatic pressure distribution can be considered as a good approximation to the actual pressure distribution in the vertical for the pure channel expansion.

(a)

(b)

(c)
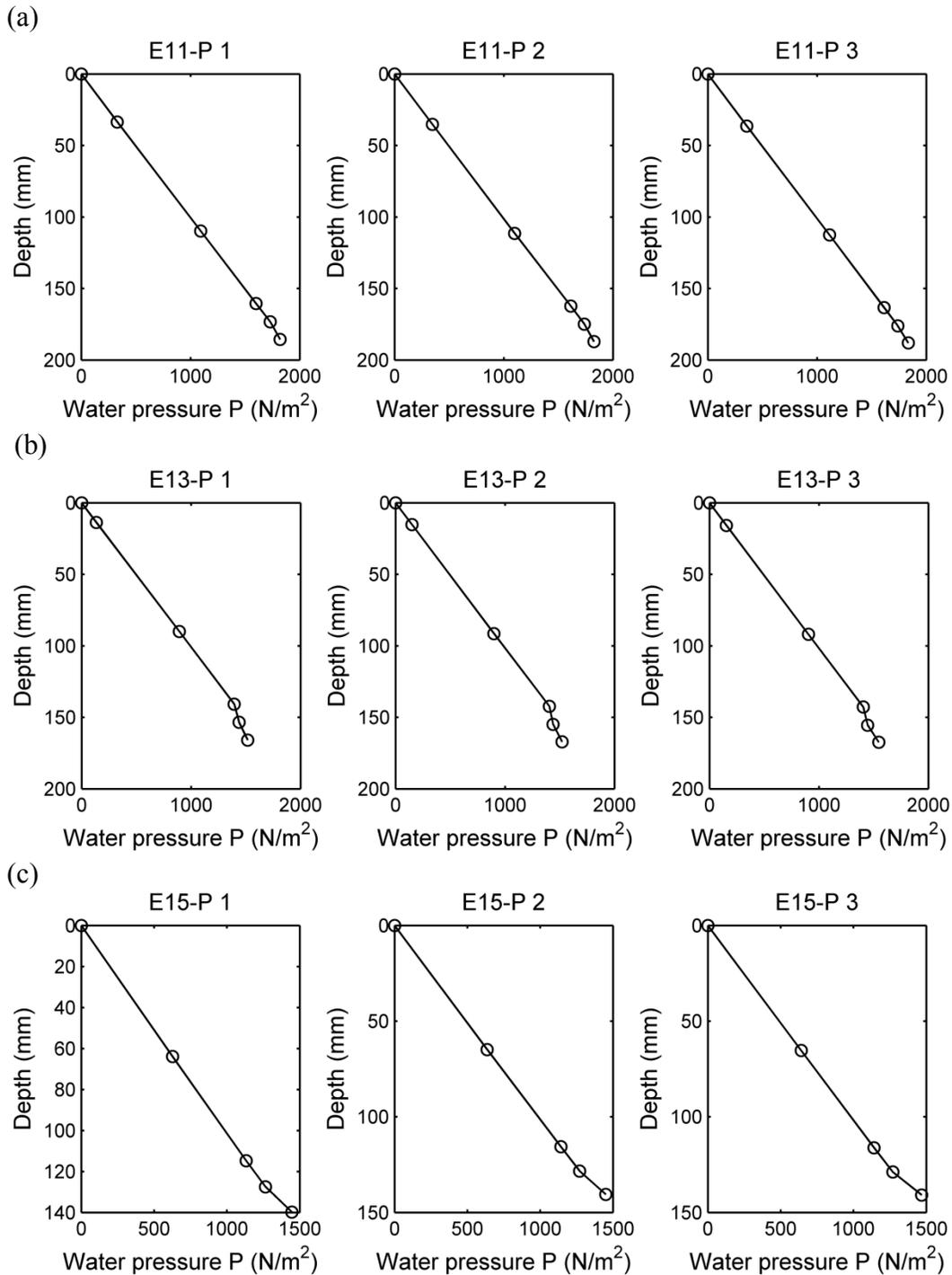
Figure 5.6   Measured pressures varying with depth below the water surface. The top, middle and bottom panels are for experiments E11, E13 and E15, respectively. For each of the experiments, P1, P2 and P3 correspond to pressure taps A1–Z1, A2–Z2, and A3–Z3, respectively.
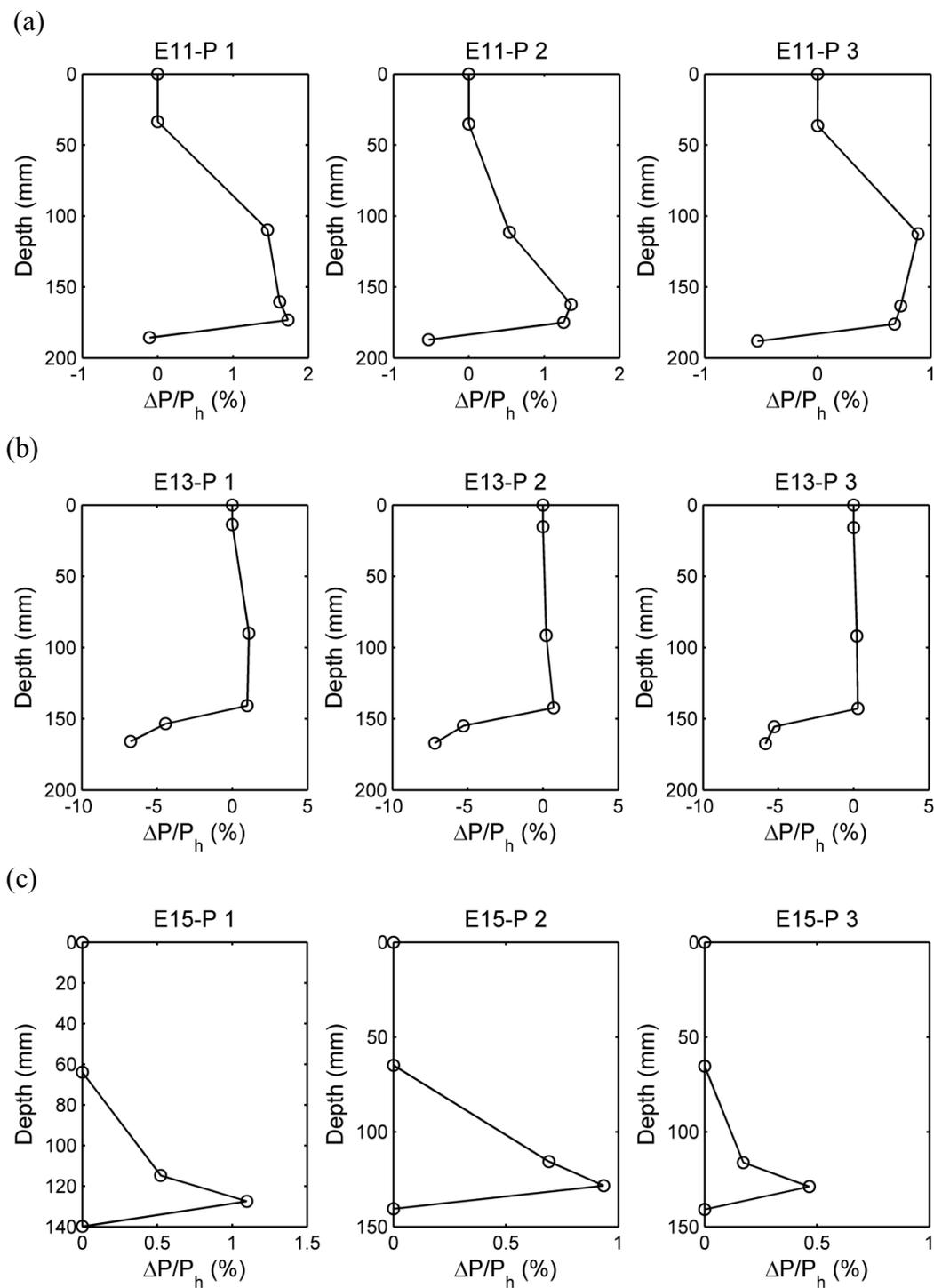
Figure 5.7   Deviations of the measured pressures from the hydrostat pressure values.

Other descriptions are identical to Figure 5.6.

5.8   Pressure force on the sidewalls

The force that each of the two sidewalls of the expansion exerts on the flowing water can be obtained by integrating the pressure over the sidewall's area, *R*, i.e.

$$F_w = \iint_R p\,dA \qquad (5.7)$$

where *dA* is the area element of the integration region. This integral needs to be approximated by a finite summation over subdivided vertical strips. An example of this summation approximation is shown in Figure 5.8 for experiment E11. The strips are divided by straight vertical lines through the middle of adjacent pressure taps.
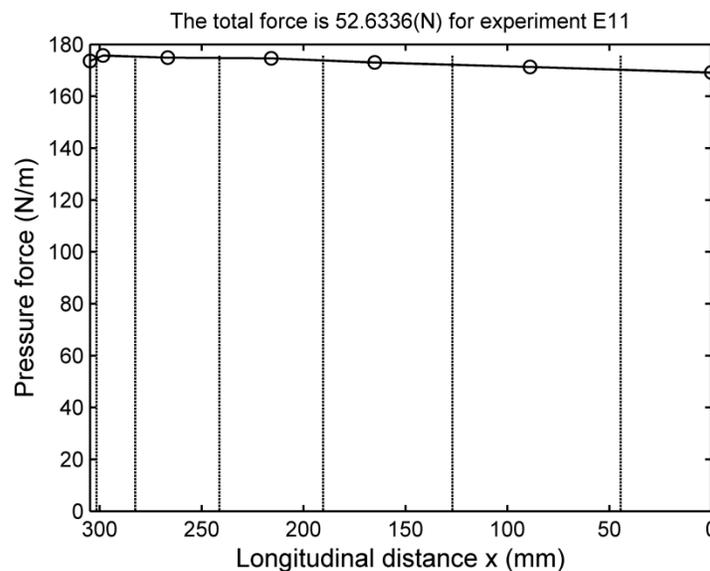
Figure 5.8   Subdivided areas for the calculation of the pressure force on the sidewall of the expansion. The sidewall force for experiment E11 is $F_w = 52.6$ N.

The forces exerted by the sidewall on the flowing water have been calculated for all the experiments. It has been assumed that the forces exerted by the two sidewalls are equal in the application of the momentum concept. For experiments E11 throughout E16 the forces are 52.63,

51.71, 40.54, 34.69, 29.58 and 19.80 N, respectively. What is more interesting is to further find $\eta(\xi)^2$ in the mean value theorem for definite integrals [see Equations (3.11) and (3.12)]. Notice that $\eta(\xi)^2$ represents the average value that the depth of flow squared $\eta^2(x)$ takes at one or more points $x = \xi$ in the x interval [0, 323.3] mm of the expansion (see Table 4.1).

$$\eta(\xi) = \sqrt{\frac{2\cos(\alpha/2)F_w}{\gamma}L_2} \tag{5.8}$$

η may also be referred to as the water surface measured above the channel bottom.

The dimensionless form η^* can be calculated from dividing η by the depth of flow at CS2 (see Equation (3.16c)], ranging from 1.00 to 1.06 for experiments E11 to E16. Once η^* is known, calculations for the depth of flow at CS3 or y_3 and hence the coefficient of energy losses for the expansion can be done. When η^* is as large as 1.06, k_E has negative values, which is unphysical. One possible explanation for the unphysical results is that some physical processes have caused energy losses but have not been allowed for in the theory presented in Chapter 3.

Chapter Six   Results for Experiments with a Hump

6.1   Introduction

The preceding chapter has discussed the results for the experiments with a flat-bottom expansion. In this chapter, an extra hump is incorporated on the bottom of the expansion. The conditions of new experiments with the hump are described in Section 6.2. Section 6.3 provides a comparison of the energy loss coefficient between experiments of subcritical flow in the expansion with and without the hump. An adverse pressure gradient is responsible for flow separation and turbulent eddy motion. Section 6.4 discusses the role that the hump plays in pressure distributions in the direction of flow. Given the possibility that the flow pattern is asymmetric relative to the expansion geometry, the distributed pressures on the two sidewalls of the expansion are examined in Section 6.5. The purpose is to show the similarity of water pressures between the two sidewalls.

6.2   Experimental Conditions

A total of 10 experiments were conducted with a hump incorporated on the bottom of a gradual expansion (Figure 3.4). This expansion has the same horizontal dimensions (Table 4.1) as the one used for the experiments (Table 5.2) described in Chapter 5. The hump has a crest height of $\delta = 0.5$ inches. The conditions of the 10 experiments (H25–H34) are described in Table 6.1. The range of discharges is from $Q = 11.80$ to 12.76 L/s. These Q values were obtained from measurements using the 30° V-notch weir (Figure 4.4). The discharge was controlled by a valve of the pumping system (Figure 4.1). The average discharge is 12.20 L/s. Verifications of the V-notch discharge measurements have been shown in Figure 5.1.

For each of the 10 experiments listed in Table 6.1, the upstream depth of flow y_1 was measured in two different ways. One way was that the depth was obtained from the difference between the initial reading (the channel bottom) and the final reading (the water surface) of a point gauge. The precision of the point gauge is 0.1 mm. The other way was that a scale tape was used to directly measure the depth. The tape had a lower precision, but measuring the depth in two different ways was for verification purposes. The range of the upstream depth of flow is from 14.78 to 24.58 cm, and the average is 19.53 cm. The depth was controlled by the downstream gate (Figure 4.3).

The ratio of the hump's crest height to the upstream flow depth, δ/y_1, has values between 0.052 and 0.086. The average value is 0.067. If the ratio is too high, it is possible that the approaching flow is choked by the hump. Such a condition must be avoided.

Table 6.1   Conditions of the experiments with a hump fitted on the bottom. The water temperature was $T = 22.5°C$.

Experiment	Q (L/s)	y_1 (cm)	δ/y_1	v_1 (cm/s)	Fr_1	Re
H26	11.80	24.58	0.052	28.07	0.18	185995
H25	11.80	23.86	0.053	28.92	0.19	187443
H27	11.80	22.27	0.057	30.98	0.21	190966
H28	12.64	21.24	0.060	34.78	0.24	207255
H29	12.64	19.40	0.065	38.09	0.28	212918
H30	12.64	18.33	0.069	40.31	0.30	216709
H31	11.80	17.27	0.074	39.95	0.31	206312
H33	12.76	17.18	0.074	43.43	0.33	223476
H34	12.15	16.36	0.078	43.44	0.34	216422
H32	11.92	14.78	0.086	47.16	0.39	220003

At the upstream cross section of the experimental channel (Figure 3.4), the maximum value for the flow velocity is v_1 = 47.16 cm/s. The upstream velocity (v_1) has been calculated by dividing the discharge by the cross-sectional area at upstream [Equation (3.16a)]. In order to smooth out small surface waves, which disturbed the flow in some of the experiments, point-gauge measurements were obtained at up to four points across the width of the channel. The average velocity at the upstream cross section is 37.51 cm/s. The minimum velocity is 28.07 cm/s. For all the experiments, the flow was subcritical, with the Froude number (Fr) less than one. The actual values for the Froude number varied from 0.18 to 0.39. The Froude number is calculated using Equation (3.9).

For all the experiments, the Reynolds number (Re) was kept at high values (Table 6.1). Thus, the flow was fully turbulent, with negligible viscous effects. This is important as the focus of the present study is on expansion losses. The average Reynolds number is 206750, and the lower and upper limits are 185995 and 220003, respectively. The Reynolds number is given in Equation (5.2).

6.3   Measured Energy Loss Coefficients

The flow energy lost in the expansion with the hump has been determined for experiments H25–H34 (Table 6.1), following the procedures described in Section 5.4. The energy loss coefficient k_E values for the experiments are plotted in Figure 6.1. For comparison purposes, the k_E values for the experiments without the hump (Table 5.2) are also plotted in the figure.

Clearly, the k_E values for the experiments with the hump are plotted below those for the experiments without the hump. Specifically, because of the presence of the hump, the energy loss coefficient drops from the 0.46–0.62 range to the 0.06–0.29 range. Notice that the two sets

of experiments have similar values for the Froude number, ranging from 0.24 to 0.43 for the experiments without the hump, and ranging from 0.18 to 0.39 for the experiments with the hump. The Reynolds number has similar values as well. The hump helps suppress flow separation and associated turbulent eddy formation that is known to dissipate energy in the flow.

Among the 10 experiments listed in Table 6.1, the experiment H32 has produced the lowest energy loss coefficient. This particular experiment had the highest Froude number; surface waves disturbed the flow and resulted in errors in measurements. For this reason, the energy loss coefficient for experiment H32 seems unrealistic.
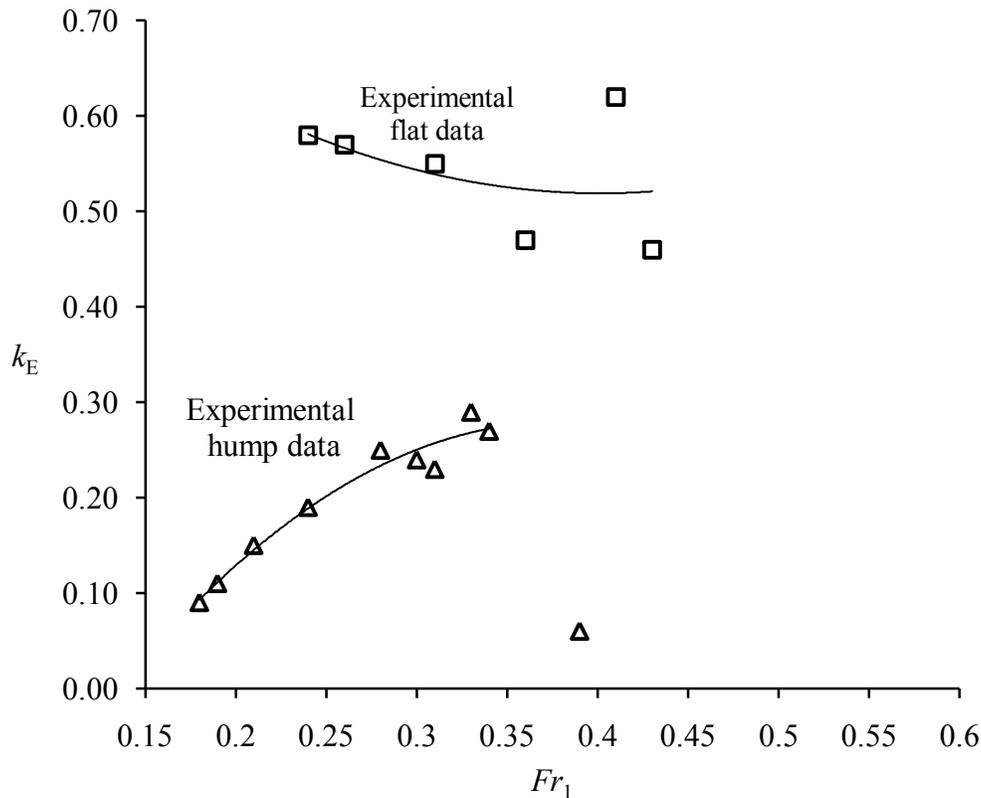
Figure 6.1   Energy loss coefficients (indicated by the symbol Δ) for the experiments with the hump. The energy loss coefficients (indicated by the symbol □) for the experiments without the hump are plotted for comparison.

6.4   Pressure Gradient in the Direction of Flow

The water pressure gradient in the direction of flow, $\dfrac{dp}{dx}$, is one of the most important factors

that determine the behaviour of flow, particularly flow separation from the solid sidewalls of a

channel expansion. In the expansion there are 45 pressure openings, with 20 drilled through each

of the two sidewalls and 5 through the channel bottom (Figure 4.2). The positions of the pressure

openings are shown in Figure 6.2. For each of the 10 experiments listed in Table 6.1, the

pressure gradient between every parity adjacent pressure openings along each row of pressure

openings is calculated. The pressure gradient is taken as the difference in pressure between the

two openings, Δp, divided by the distance between them, ΔL. Since the pressure opening rows

are not horizontal but tilt up by a small angle of $\varepsilon = 2.54°$ from the horizontal direction, the

pressure gradient is resolved into the horizontal direction as

$$\frac{dp}{dx} \approx \frac{\Delta p}{\Delta L}\cos\varepsilon \qquad\qquad (6.1)$$
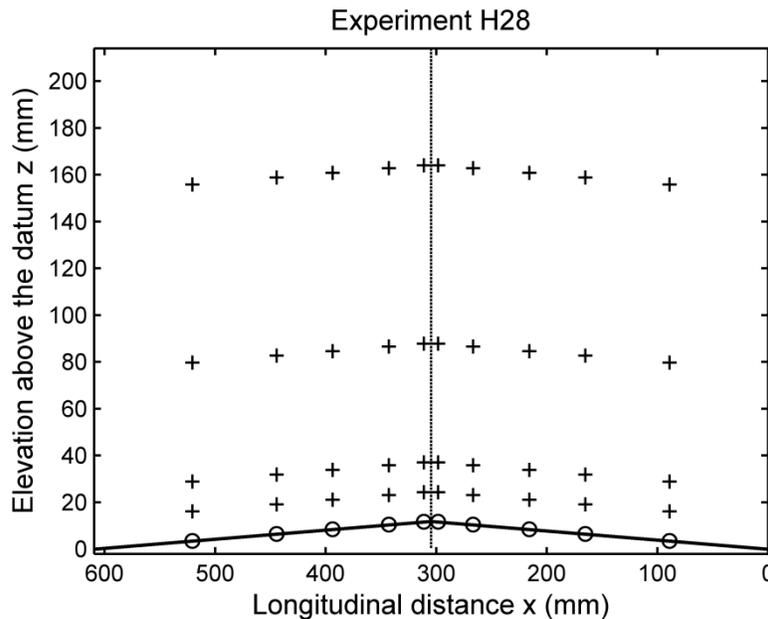
Figure 6.2   Positions of the pressure openings. The expansion is

between $x = 0$ and $x = 323.3$ mm

The pressure gradient given in Equation (6.1) varies from point to point along each row of pressure openings, becoming the strongest at a certain point (Table 6.2). Notice that A1–A5 represents the five pressure openings (from upstream to downstream; hereafter the same sequent order) on the top row. B1–B5 corresponds to the five pressure openings on the second row from the top. C1–C5 symbolises the five pressure openings on the third row from the top. D1–D5 denotes the five pressure openings on the fourth row from the top. Z1–Z5 represents the five pressure openings on the channel bottom.

The negative values for the pressure gradient shown in Table 6.2 mean that the pressure drops in the direction of the flow. The adverse pressure gradients shown in Table 5.2 for the experiments with a flat bottom have been converted into favourable pressure gradients by the hump for all the experiments listed in Table 6.1, except for experiment H32. This experimental evidence suggests that flow separation has been suppressed if not eliminated completely.

Table 6.2 The strongest pressure gradient along each row of the pressure openings for experiments H25 to H34, listed in Table 6.1.

Experiment	Minimum Pressure gradient				
	A1-A5	B1-B5	C1-C5	D1-D5	Z1-Z5
H25	-0.037	-0.047	-0.047	-0.043	-0.089
H26	-0.037	-0.043	-0.047	-0.051	-0.05
H27	-0.052	-0.036	-0.047	-0.032	-0.085
H28	-0.046	-0.036	-0.051	-0.032	-0.074
H29	-0.033	-0.047	-0.051	-0.032	-0.082
H30	-0.036	-0.037	-0.059	-0.043	-0.082
H31	-0.043	-0.037	-0.059	-0.043	-0.0698
H32	□	-0.032	-0.051	-0.047	-0.074
H33	-0.051	-0.037	-0.055	-0.055	-0.074
H34	-0.036	-0.034	-0.043	-0.047	-0.074

6.5   Distribution of Pressure Forces on the Sidewalls

Application of the momentum principle entails the evaluation of all the forces, including the pressure forces exerted by the two sidewalls of the expansion on the flowing water. The pressure openings are symmetric between the two sidewalls. It would be interesting to exam to what extent the pressure distributions on the two sidewalls are symmetric. For this purpose, the pressures measured at the corresponding openings on the two sidewalls are shown in Figure 6.3. The data are plotted virtually through the straight diagonal line, meaning that the pressure distributions are indeed symmetric. In other words, if two points, one on each of the two sidewalls, are at the same elevation about the channel bottom and the same distance from the inlet of the expansion, the pressures at the two points are equal. Due to disturbances from surface, there are a very small number of exceptions.

To further confirm this symmetric feature of the pressure distributions, a correlation analysis is carried out. Let p_L and p_R denote the pressures measured at the corresponding pressure openings on the sidewall to the left and to the right (facing downstream), respectively. The correlation between p_L and p_R may be expressed as

$$Correl(p_L, p_R) = \frac{\sum (p_L - \bar{p}_L)(p_R - \bar{p}_R)}{\sqrt{\sum (p_L - \bar{p}_L)^2 \sum (p_R - \bar{p}_R)^2}} \qquad (6.2)$$

When all the individual pressure openings for all the experiments listed in Table 6.1 are included, there are 191 pressure data records. They are perfectly correlated, with a correlation coefficient of as high as 0.999 [Equation (6.2)]. Thus, for the purpose of determining the pressure forces, it is sufficient to obtain pressures on one sidewall.

The total forces acting on the fluid element in the expansion have been evaluated for all the experiments listed in Table 6.1. The dimensionless parameter η^* [Equations (3.13) and

(3.18c)] has values in the range of 0.96 to 0.99 for all the experiments, except experiment H32 (Table 6.1) for which the parameter is 1.13. This parameter value is unrealistic. The forces are used to determine the theoretical values for the depth of flow y_3 at the outlet of the expansion for all the experiments. The computational procedures are similar to those followed in Chapter 5. In comparison with the measured y_3 values for the experiments (Table 6.1), the theoretical values contain errors of 6% on average.
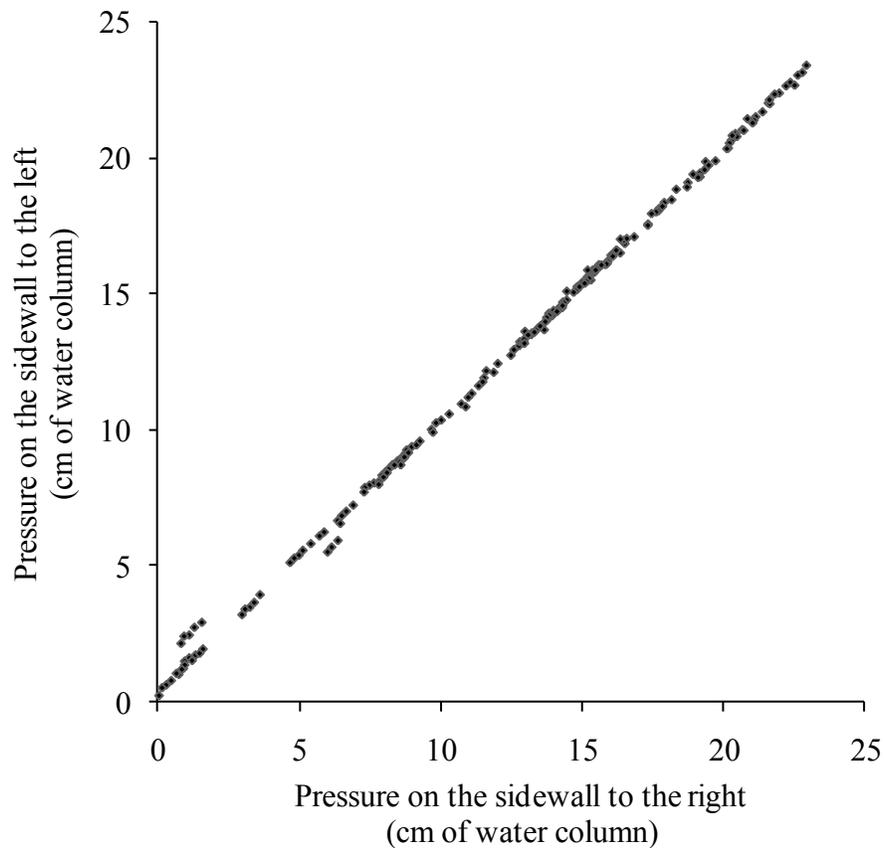
Figure 6.3 Comparison between water pressures measured at corresponding pressures openings through the sidewall to the left and the sidewall to the right (facing downstream). The pressure is expressed in height (cm) of water column.

Chapter Seven　　　Discussion and Conclusion

7.1　　Discussion

Sudden expansions are perhaps easy to build but are known to give a poor hydraulic performance. Accordingly, the energy loss coefficient k_E for a sudden expansion will have higher values than a gradual expansion of the same dimension. This expected result has not been predicted by the formula for k_E of Henderson (1966). The formula is intended for a sudden expansion; it is expected to produce k_E values higher than the experimental k_E values for the gradual expansion. However, it produces the opposite effect (Figure 5.2). This means that the formula of Henderson (1966) has underestimated the flow energy lost in a sudden expansion; possibly, the assumption that Fr_1 is small enough for Fr_1^4 and higher powers to be neglected is invalid.

It is logical that the hydraulic performance of expansions can be improved by proper modifications to their geometry in the horizontal or in the vertical or in both dimensions. The effectiveness of horizontal modifications is inconclusive; inconsistent experimental evidence has been reported in the literature (e.g. Hinds 1927; Smith and Yu 1966; Swamee and Basak 1992). Vertical modifications represent a good alternative. This study has produced experimental evidence that the incorporation of a simple hump onto the channel bottom of an expansion is able to make desirable changes to water surface profiles in the expansion. In a flat-bottom expansion, water-surface profiles have positive slopes (about 1%) in the direction of flow (Experiments E11 to E16 in Table 5.1), which tend to trigger flow separation. Such a tendency is suppressed by the presence of the hump.

There is no doubt that experimental measurements are essential for the design of expansions. Nevertheless, it is not always possible to simultaneously ensure all relevant hydraulic similarities (Houghtalen et al. 2010). Besides, laboratory experiments are expensive and time-consuming to carry out. Thus, theoretical analyses play an important supplementary role. In this regard, the present study has made a contribution by formulating the energy behaviour of flow in expansions. This formulation would be useful for the optimisation of expansion parameters and for the design of laboratory experiments of subcritical flow in expansions.

Several empirical formulae have been suggested for estimates of the energy head loss in an expansion. Chow (1959, page 464–468) summarised Formica's experimental results of subcritical flow through sudden expansions, and estimated the head loss from $h_L = C_L (\Delta v)^2 / 2g$ where C_L is a coefficient and Δv is the change in velocities between the inlet and outlet of the expansion. This formula is similar to the head loss due to sudden enlargement in a pipe, given by $h_L = (\Delta v)^2 / 2g$ (Houghtalen et al. 2010). The above expressions can be derived from the momentum considerations (see e.g. Daugherty and Franzini 1977). Another way to express the head loss is a coefficient, k_E, times the change in velocity head between the inlet and outlet of the expansion, i.e. $h_L = k_E (v_2^2 - v_3^2) / 2g$ (see e.g. Morris and Wiggert 1972. This expression is the same as the expression for the energy head in a pipe diffuser, where the diffuser angle determines the coefficient k_E (Houghtalen et al. 2010). In the special case where turbulent flow passes through a horizontal pipe, with its cross-sectional area enlarged suddenly from A_2 to A_3, the energy loss in the expansion is given by the Borda-Carnot relationship of the form $h_L = (1 - A_{21} / A_3)^2 v_2^2 / 2g$ (see e.g. Douglas et al., 2005, p. 354). Obviously, the energy loss

coefficients in the above-mentioned different expressions will have different values, and may lead to confusion.

In this study, the energy loss formulation is according to Equation (3.22b). Here, an emphasis is given to the difference in k_E between the case of a flat-bottom expansion and the case of the expansion with an extra hump. The median values for k_E are 0.56 and 0.23 for the former and latter cases. The difference of 0.33 may be interpreted as the coefficient of energy head saving from using the hump. To demonstrate the significance of this saving, numerical sample calculations are provided below.

Consider the design case of a trapezoidal expansion given in Vittal and Chiranjeevi (1983). The total discharge is $Q = 357$ m³/s. The side slope of the trapezoidal section is 1:2 (Vertical:Horizontal) or $m = 2$. The bottom width of the section is $b = 23$ m. The Manning's coefficient is taken as $n = 0.022$ (typical value for natural channels, Chow 1959). The longitudinal slope of the natural channel bed $S_o = 0.002$ (typical value). For these give conditions, the normal depth y_n can be obtained from the Manning's equation (S.I. unit) for uniform flow

$$\frac{Q}{A} = \frac{1}{n} R_h^{2/3} S_o^{1/2} \tag{7.1}$$

where A is the cross-sectional area, given by $A = (b + my_n)y_n$, and R_h is the hydraulic radius, given by $R_h = (b + my_n)y_n / \left(b + 2\sqrt{y_n^2 + (my_n)^2} \right)$. The value for y_n is 3.21 m. The flow area is $A = 94.44$ (m²). The top width is $T = 36.88$ (m). The corresponding hydraulic depth is $D = 2.56$ (m). The cross-sectional mean velocity is $V = 3.78$ (m/s). The Froude number is $Fr = 0.75$. This

means the flow is subcritical. The energy head saving, given by $\Delta H = 0.33 \dfrac{(Q/A)^2}{2g}$, will be

22.13 (m). The corresponding power saved will be 227 (kWatt).

7.2   Concluding Remarks

In this study laboratory experiments have been conducted to investigate the energy behaviour of

open-channel flow in expansions. A theoretical formulation of the flow energy has also been

derived from the momentum and energy principles. The flow in the experiments is subcritical,

with the Froude number in the range of 0.18 to 0.43, and is turbulent, with the Reynolds number

ranging from 1.85×10^5 to 2.48×10^5. The measurements produced from the experiments include

the depth of flow, distributed pressure and discharge, which are of good quality. Analyses of the

experimental and theoretical results lead to the following conclusion.

(1)   A hump fitted onto the channel bottom of an expansion is effective at enhancing the

recovery of flow energy head. The mechanics of head recovery is such that the otherwise

adverse pressure gradient is converted to favourable pressure gradient by the hump. This

conversion inhibits the occurrence of flow separation and the formation of energy-

dissipating turbulent eddies. From the flow energy perspective, the presence of the hump

promotes the transfer of kinetic to potential energy, as the flow passes over the hump.

Part of the flow energy is forced to preserve as elevation head, a source available for the

downstream.

(2)   From the kinetic point of view, the vertical geometric feature of a hump causes the flow

to accelerate, and neutralises the decelerating effects of the expanding width in the

horizontal. This is clear from the changes in cross-sectional area derived from flow depth

measurements.

(3)   The usefulness of a hump can be quantified using the head recovery coefficient, defined as $1 - k_E$. With a flat-bottom expansion, the energy head recovery is at the level of 44% (the median value) of the approaching flow velocity head. By installing the extra hump, the head recovery is increased to the level of 77%. Given the simplicity of such a hump, it is considered a great advantage over an expensive optimisation of expansion geometry in the horizontal. The performance improvement of the optimisation is not even conclusive.

(4)   For the purpose of expansion design, theoretical calculations of flow energy recovery can be done by combining the momentum and energy principles, following a simplified procedure. First, the pressure forces at the inlet and outlet of the expansion can be evaluated using the hydrostatic approximations. Experimental data show that the errors of such approximations are typically 5% or lower. The depths required as input are easy to measure. Secondly, the pressures at two corresponding positions on the two sidewalls of the expansion are perfectly symmetric, with a correlation coefficient of as high as 0.999, and therefore it is sufficient to evaluate the pressure force on only one sidewall. Third, to evaluate this sidewall pressure force, the depth at the inlet of the expansion can be used, together with a scale-up factor (η^*). Empirical values for this scale-up factor have been obtained.

(5)   Theoretical values for the depth of flow at the outlet of the expansion and for the energy loss coefficient are in reasonable agreement with the experimental data. One of the experimental challenges is the control of disturbances caused by water surface waves to the flow in the expansion, which become severe when the Froude number exceeds 0.4.

Fortunately, it has been shown that the Froude number does not have a strong influence on the flow energy behaviour.

7.3   Suggestion for Future Research

The present study has assumed that the flow velocities at the inlet to the expansions are uniform. Future studies should consider the influence of distributed flow velocities at the inlet, and remove the assumption that the energy coefficient is unity. For this purpose distributed flow velocities at selective cross sections in expansions need to be measured. Future studies should also investigate the effects of expansions of different dimensions and configurations on flow behaviour. For this purpose, the dual approach of combining laboratory experiments with numerical modelling would be effective. With experimental data available for calibration and validation, numerical modelling of flow behaviour in expansions using CFD code is a worthy undertaking.

References

Abbott, D. E., and Kline, S. J. (1962). "Experimental investigation of subsonic turbulent flow over single and double backward facing steps." *Journal of Basic Engineering 84,* 317.

Babarrutsi, S., Ganoulis, J., and Chu, V. H. (1989). "Experimental investigation of shallow recirculating flows." *Journal of Hydraulic Engineering* 115(7), 906–924.

Babarrutsi, S., and Chu, V. H. (1991). "Dye-concentration distribution in shallow recirculating flows." *Journal of Hydraulic Engineering* 117(5), 643–659.

Bos, M. G. (1989). "Discharge measurement structures" 3rd edition. ILRI publication 20, ILRI, Wageningen.

Chow, V. T. (1959). "Open-channel hydraulics." McGraw-Hill Bok company, N.Y.

Daugherty, R. L., and Franzini, J. B. (1977). "Fluid mechanics with engineering applications." McGraw-Hill Book Co., N.Y.

Dey, S. (1998). "Choke-free flow in circular channels with increase in bed elevations." *Journal of Irrigation and Drainage Engineering* – ASCE 124(6), 317–320.

Douglas, J. F., Gasiorek, J. M., Swaffield, J. A., and Jack, J. B. (2005). "Fluid mechanics." 5 edition. Prentice-Hall, Harlow, England.

Escudier, M. P., Oliveira, P. J., Poole, R. J. (2002). "Turbulent flow through a plane sudden expansion of modest aspect ratio." *Journal of Physics of Fluids* – AIP 14(10), 3641–3654.

Foumeny, E. A, Ingham, D. B, and Walker, A. J. (1996). "Bifurcations of incompressible flow through plane symmetric channel expansions." *Journal of Computers and Fluids* 25(3), 335–351.

Graber, S. D. (1982). "Asymmetric flow in symmetric expansions." *Journal of the Hydraulics Division* – ASCE 108(HY10), 1082–1101.

Houghtalen, R. J., Akan, A. O., and Hwang, N. H. C. (2010). "Fundamentals of hydraulic engineering systems." 4th edition. Prentice-Hall, Inc., Upper Saddle River, NJ 07458.

Henderson, F. M. (1966). "Open channel flow." Prentice-Hall, Inc., Upper Saddle River, NJ 07458.

Hinds, J. (1927). "The hydraulic design of flume and siphon transitions." *Proceedings of the American Society of Civil Engineers* Paper No.1690, 1423–1459.

Ingram, R. G., and Chu, V. H. (1987). "Flows around islands in Rupert Bay: An investigation of the bed-friction effect." *Journal of Geophysical Research–Ocean* 92(C13), 14521–14534.

Kalinske, A. A. (1944). "Conversion of kinetic to potential energy in flow expansions." Transactions–American Society of Civil Engineers, Paper No. 2273, 355–390.

Kindsvater, C.E, and Carter, R.W. (1957). "Discharge characteristics of rectangular thin-plate weirs." *Journal of the Hydraulics Division* – ASCE 83(6), 1–36.

Liong, S. Y. (1984). "Channel design and flow operation without choke." *Journal of Irrigation and Drainage Engineering* – ASCE 110(4), 403–407.

Mazumder, K. M., and Hager, W. H. (1993). "Supercritical expansion flow in rouse modified and reversed transitions." *Journal of Hydraulic Engineering* 119(2), 201–219.

Mehta, P. R. (1979). "Flow characteristics in tow-dimensional expansions." *Journal of the Hydraulics Division* – ASCE 105(HY5), 501–516.

Mehta, P. R. (1981). "Separated flow through large sudden expansions." *Journal of the Hydraulics Division* – ASCE 107(HY4), 451–460.

Mohapatra, P. K., and Bhalamudi, S. M. (1994). "Bed-level variation in channel expansions with movable beds." *Journal of Irrigation and Drainage Engineering* – ASCE 120(6), 1114–1121.

Morris, H. M., and Wiggert, J. M. (1972). "Applied hydraulics in engineering." 2nd edition. The Ronald Press Company, N.Y.

Nashta, C. F., and Grade, R. J. (1988). "Subcritical flow in rigid-bed open channel expansions." *Journal of Hydraulic Research* 26(1), 49–65.

Papanicolaou, A., and Hilldale, R. (2002). "Turbulence characteristics in a gradual channel transition." *Journal of Engineering Mechanics* 128(9), 948-960.

Ramamurthy, A. S., Basak, S., Rao, P. R. (1970). "Open channel expansions fitted with local hump." journal of hydraulics division – ASCE 96(HY5), 1105–1113.

Reneau, R. L., Johnston, J. P., and Kline, S. J. (1967). "Performance and design of straight, two-dimensional diffusers." *Journal of Basic Engineering–Transactions of the ASME*, March, 141–150.

Seetharamiah, K., and Ramamurthy, A. S. (1968). "Triangular sills in open channel expansions." *Civil Engineering and Public Works Review* 63, March, 283.

Skogerboe, G. V., Austin, L. H., and Bennett, R. S. (1971). "Energy loss analysis for open channel expansions." *Journal of the Hydraulics Division*–ASCE 97(HY10), 1719–1735.

Smith, C. D., and Yu, J. N. G. (1966). "Use of baffles in open channel expansions." *Journal of the Hydraulics Division*–ASCE 92(HY2), 1–17.

Swamee, P. K., and Basak, B. C. (1991). "Design of rectangular open-channel expansion transitions." *Journal of Irrigation and Drainage Engineering* – ASCE 117(6), 827–838.

Swamee, P. K., and Basak, B. C. (1992). "Design of trapezoidal expansive transitions." *Journal of Irrigation and Drainage Engineering* – ASCE 118(1), 61 – 73.

Swamee, P. K., and Basak, B. C. (1993). "Comprehensive Open-Channel Expansion Transition Design." *Journal of Irrigation and Drainage Engineering* – ASCE 119(1), 1–17.

U.S. Department of Transportation (1983). "Hydraulic design of energy dissipators for culverts and channels." *Hydraulic Engineering Circular* Number 14, Third Edition.

Vittal, N., and Chiranjeevi, V. V. (1983). "Open channel transitions: rational method of design." *Journal of Hydraulic Engineering* – ASCE 109 (1), 99–115.

White, F. M. (2006). "Viscous Fluid Flow." 3rd edition. McGraw-Hill, N.Y.